## ABSTRACT

NOEVERE, ALEXANDER M. Survivability of Optical Fibers with Fiber Bragg Gratings During Soft Body Armor Testing. (Under the direction of Dr. Mark Pankow).

Ballistics fabrics, such as Kevlar® are commonly used today to create personal protective systems capable of withstanding direct impact from firearm projectiles. The current National Institute of Justice (NIJ) standard for personal body armors is lacking in the fact that it does not consider any time dependent data regarding the deformation and instead relies on measuring the plastic deformation within the backing material after impact. Through the use of Fiber Bragg Gratings (FBG's), it is possible to gather time dependent information regarding the deformation. However, due to the hostile environment present during a ballistic impact test, additional protection is needed for the FBG to ensure it survives projectile impact.

A high-pressure gas gun was used to fire projectiles into ballistic fabric systems consisting of multiple layers of Kevlar® KM2® Plus. The armor systems were placed against backing material testing blocks consisting of either 20% NATO standard ballistics gelatin or Roma Plastilina #1 modeling clay. Sensing layer mats which served to protect the FBG during impact were then placed between the armor system and backing material. Using a combination of structure scanners and high-speed cameras, it was possible to gather information regarding the deformation depth, width, and volume.

The sensing layers were fabricated out of different materials to study how each material affected the deformation dimensions during impact as well as how effective each was at preventing the attached FBG from fracturing during impact. It was found that fibers which were cast into silicone sensing layers had the highest likelihood of surviving impact while fibers which were stitched onto a sheet of Kevlar® fabric performed poorly once projectile velocity was increased to match the current NIJ Type IIIA testing standard. It was also observed that the

sensing layer thickness had a significant effect on the final deformation dimensions of the backing material, as the use of a 2mm thick silicone sensing layer saw a noticeable reduction in deformation depth and volume. Overall, a 1mm thick, transparent silicone sensing layer proved to be the optimal balance between ensuring the FBG's protection and minimizing any impact on the deformation dimensions.

# Survivability of Optical Fibers with Fiber Bragg Gratings During Soft Body Armor Testing

by
Alexander M Noevere

A thesis submitted to the Graduate Faculty of
North Carolina State University
in partial fulfillment of the
requirements for the degree of
Master of Science

Mechanical Engineering

Raleigh, North Carolina

2018

APPROVED BY:

| | |
|---|---|
| _____ | _____ |
| Dr. Scott Ferguson | Dr. Kara Peters |

_____
Dr. Mark Pankow
Committee Chair

## DEDICATION

I dedicate this to my parents, Eric and Michelle, and to my partner/best friend, Taylor.

## BIOGRAPHY

Alexander Noevere graduated with a Bachelor of Science degree in Mechanical Engineering from North Carolina State University (NCSU) in May, 2016. During the course of his undergraduate career he completed several internships with NAVAIR, working at the Cherry Point Air Station in Havelock, NC. There he started to develop an interest in aerospace structures, specifically advanced composite structures. Upon receiving his Bachelor's degree from NCSU, Alex was offered the Graduate Merit Award to pursue his Master's degree in Mechanical Engineering at NCSU. While transitioning into graduate school, he completed a summer internship at Honda Aircraft Company LLC. Because of his experiences at Honda Aircraft, he decided to study the field of Mechanics of Materials, with an emphasis on composite materials.

## ACKNOWLEDGMENTS

I would like to thank my advisor, Dr. Mark Pankow for all of his help and guidance during my years as both an undergraduate and graduate student. Thank you also to Dr. Scott Ferguson and Dr. Kara Peters for agreeing to serve on my committee. And finally, thank you to all the members of the BLAST lab for creating a fun and supportive environment which I will remember fondly for years to come.

# TABLE OF CONTENTS

# LIST OF TABLES

## LIST OF FIGURES

# CHAPTER 1 – Introduction

This chapter gives a brief overview of the body armor technology and the current state of the art in modeling and data collection. Finally, the research objectives and questions of this work will be discussed.

## 1.1 - Background

Body armor, also known as personal protective systems, has been present in the militaries of different civilizations for centuries [1]. Early body armor took the form of toughened leather panels and helmets. As material science progressed, steel replaced animal hide as the material of choice. With each new development of weaponry, personal protective systems have likewise had to adapt. The advent of modern firearms rendered most metals obsolete as a body armor material since the amount of material needed to effectively arrest a high-speed projectile would be too cumbersome for a soldier to carry on the battlefield. Today, militaries have turned to using high performance ballistic fabrics such as Kevlar® and Zylon [2]. The majority of ballistic fabrics are composed of a class of polymers known as aramids, or more specifically, para-aramids [3]. Para-aramids offer high strength properties due to the linear alignment of the polymer chains, allowing fibers spun from aramid polymers to have high strain to failure values and subsequently, strong impact resistance [3]. Ballistic fabrics can then offer exceptional tensile strength at a fraction of the weight of metals, making them advantageous for applications where weight is a critical factor.

The first ballistic fabric, Kevlar®, was developed by DuPont in 1965 and sparked the development of new personal body armor systems for military and police use [4]. These new body armors used woven pads of Kevlar®, or a similar aramid fiber, to absorb and dissipate the energy of a high velocity projectile before it could penetrate into the wearer's body and cause

internal harm. In order to ensure that new armor systems being released would provide adequate protection to individuals, the National Institute of Justice (NIJ) issued its 0101 standard, which is still in effect today. The standard examines the ability of a soft body armor system to arrest projectiles and also studies the damage caused by non-penetrating impacts [4].

During impact, the woven nature of the fabric changes the mechanisms by which energy dispersion occurs. The yarns that are directly impacted by the projectile, also known as primary or principal yarns, disperse impact energy in the form of tensile strain along the length of the yarns. The yarns which are not directly impacted, known as secondary yarns, also help with energy dispersion thanks to load transfer due to friction [5]–[7]. Figure 1 below illustrates the primary yarns during an impact from a spherical projectile.

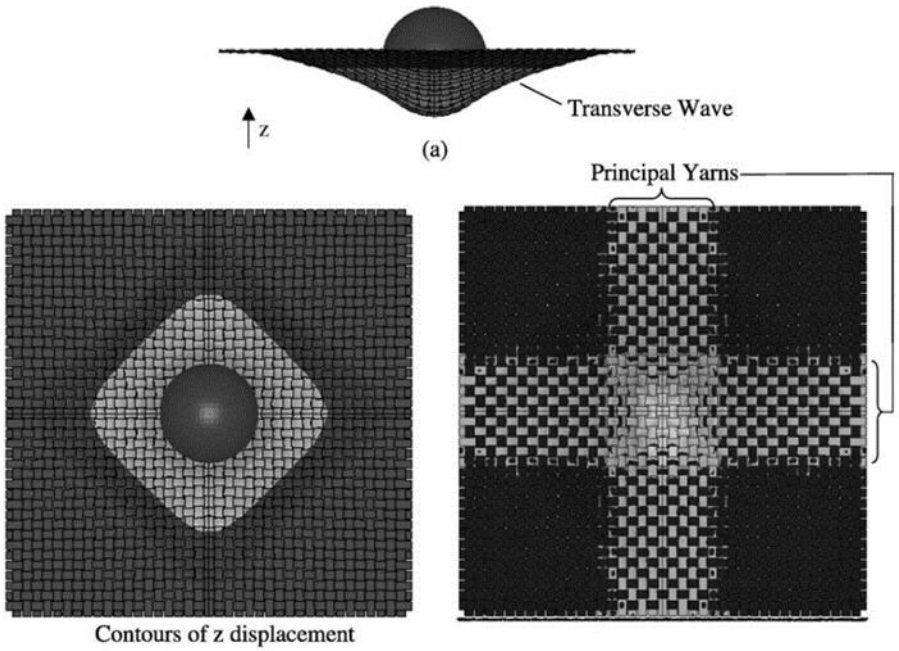


**Figure 1:** Illustration of Primary Yarns and Displacement Contour [8].

For a plain-woven fabric structure, the deformation typically produces a diamond shaped profile during the impact event, as illustrated in Figure 1. The diamond profile is due to the primary yarns being pulled tight by the projectile and in turn pulling the secondary yarns along

with them. The interactions between the primary and secondary yarns, as well as the interaction between different layers of fabric during impact has been the subject of much research in recent years and is well understood [7], [9]–[14]. However, while the mechanisms of load transfer within the armor system are well known, since the initial testing to develop the 0101 standard, there has been little research done to study the response in the backing material behind the armor pad during impact. Because of the growing concern of injury due to Behind Armor Blunt Trauma (BABT), this is a topic of increased interest [15].

Simply being able to prevent penetration of the projectile through the armor pad is not adequate to ensure the survival of the wearer. If the armor system is not effective at dissipating the kinetic energy of the projectile across a wide area, a significant amount of displacement can occur behind the armor pad, also known as Back Face Deformation (BFD). A large amount of BFD can result in BABT and possible death of the wearer [15], [16]. An ideal armor system would thus prevent penetration and excessive BABT while minimizing the overall weight of the system. In order to determine the maximum allowable BFD that could result without causing significant harm to the wearer, anesthetized goats were used as test subjects, as they had similar tissue mass in the thoracic region as a human [4]. After it became clear that Kevlar®, specifically Kevlar-29, was the most effective of the various aramid fibers at arresting projectiles, further testing was performed to study how many plies were necessary to reach a mortality risk of less than 10% [4]. Due to the desire to move away from testing on animals, new materials were studied for use as backing materials that could mimic the response of human tissue to ballistic impact. Several different materials were identified as possible candidates, including 20% ballistics gelatin and Roma Plasticina #1 and #2 modelling clay [17]. Figure 2 shows the

deformation versus time profiles of different potential backing materials. It was found that ballistics gelatin closely followed the baseline curve, determined from the goat testing data.

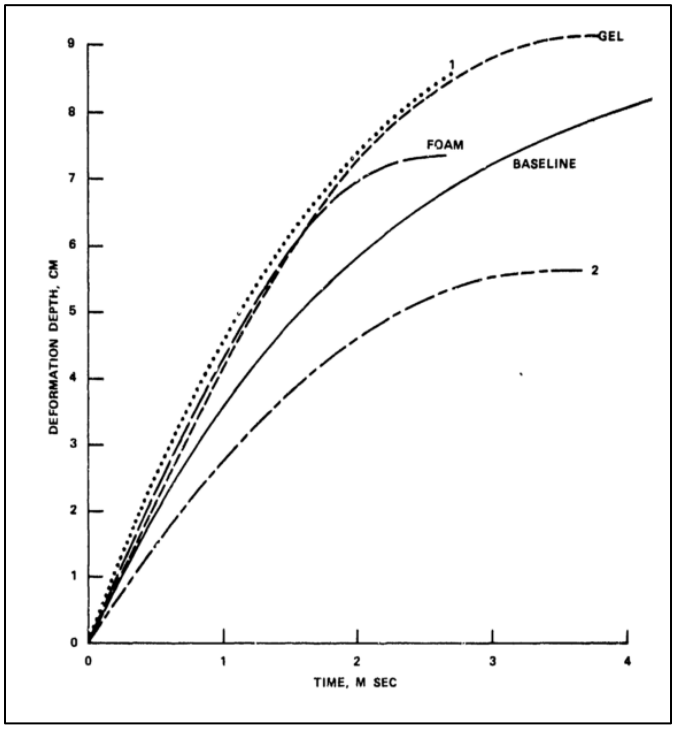


**Figure 2:** BFD Versus Time [17].

Although the ballistics gelatin provided a conservative correlation to the baseline curve, it was not desirable as a backing material since it required  a high speed camera set up, which were prohibitively expensive at the time [4]. Roma Plastilina #1 (shown as the dotted line labeled “1” in Figure 2) was selected instead since it closely followed the ballistics gelatin curve and did not recover after impact, allowing the maximum depth to be recorded without high speed cameras. It should be noted that while the use of clay as a backing material was preferable during the time that this standard was created, it has several significant disadvantages. The first is that the clay must be warmed thoroughly to approximately 110 degrees Fahrenheit in order to achieve the correct stiffness[18], depending on the size of the ballistics box used, this can take several hours. Secondly, since the clay plastically deforms during impact, only the final impact shape

dimensions can be retrieved easily. Finally, since the modeling clay does not rebound, it must be reworked each time a batch of tests is performed, or after every test if the testing block is too small to allow multiple shots. Because of this constant reworking, the clay has to be characterized frequently by measuring the depth of penetration of a 1 kilogram indenter head dropped from a height of 1 meter to ensure that the stiffness remains within acceptable limits [19].

Using the number of layers of Kevlar-29 that resulted in less than 10% mortality rate in the goats, further tests were done in ballistics gel to study the deformation depth and profile. It was found that in a ballistics gel backing material impacted with a .38 special round at 800 feet per second, the average depth of deformation was 44 millimeters [20], as shown in Figure 3. This value became the basis for the NIJ 0101 Standard, and a deformation depth of 44 millimeters is still in use as the pass/fail criterion today [19].

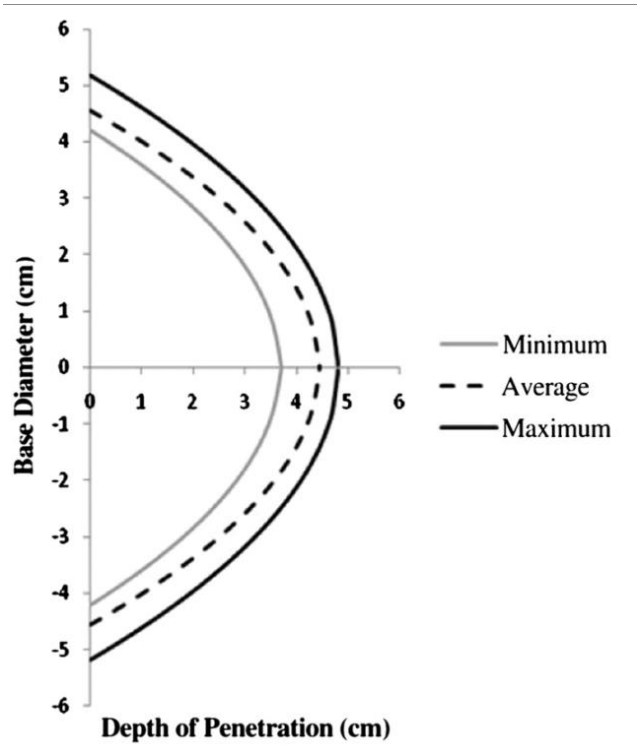


**Figure 3:** Deformation Envelope in Ballistics Gelatin [17].

The 44 mm criterion has endured due to the fact that body armor systems designed for this standard have proven to be very effective at protecting the individuals wearing it. However, there has been growing concern that the standard may be overly conservative and has resulted in unnecessarily bulky protective equipment. This is especially of interest for the military as ongoing combat operations in desert climates have raised significant concern about personnel becoming fatigued and suffering from heat exhaustion as a result of carrying around many pounds of equipment and body armor [1]. As a result, the military has begun research to develop a better understanding of how the BFD evolves over the course of a ballistic impact. This in turn will stimulate the development of the next generation of body armor which will be tailored to minimize the overall weight of the system without sacrificing its protective qualities.

In an attempt to better understand ballistic impact events when using soft body armor, many different dynamic Finite Element Models (FEM's) have been developed for ballistic fabric during a high strain rate event [6], [12], [21], [22]. These models have proven in certain cases to be able to correctly predict the V50 value or velocity at which 50% of the tests experience punch-through. However, these FEM's are still limited in many ways due to the complexity of ballistic impact events [23]. The vast majority of models produced assume a rigid projectile during simulation. In a real-world situation, the projectile will deform significantly upon impact (see Figure 4), which will undoubtedly change how the projectile energy is dispersed.

**Figure 4:** (Left) Undeformed Projectile and (Right) Projectile After Impact.

Many of these models also do not feature any type of backing material, which is an important aspect but adds further complexity. By not accounting for any type of backing material, these models are therefore incapable of predicting any type of damage done to the backing material behind the fabric. Due to this, they are unable to predict BABT due to ballistic impact, which has become a topic of increasing concern in recent years [15], [16].

All of the factors mentioned above make it nearly impossible to create a comprehensive numerical model with the current computing technology. Instead, experimental testing can be used to supplement analytical and numerical modeling techniques and develop a better understanding of the many variables and their interactions.

To fully understand how the BFD changes over time during a ballistic impact, a robust data gathering system is essential. The fabric properties of the armor system must be known beforehand as well as the velocity and mass of the projectile. In addition, time dependent information regarding the deformation of the backing material is necessary. However, accurate measurement of the area directly behind the armor system can prove to be challenging due to the harsh conditions that the measuring device is subjected to. Adding additional protection defeats the purpose of the research as the impact must simulate real-life conditions as much as possible. Many sensors typically used for direct measurements, such as metal foil strain gages or pressure

transducers, are simply too delicate to withstand the force of impact. Indirect measurements through the use of high speed cameras are possible but require a clear line of sight on the impact zone [24], something which is not feasible under the current standard which specifies modeling clay as the backing material [19].

Instead, researchers have begun using optical fibers with specially treated segments known as Fiber Bragg Gratings (FBG's). FBG's can withstand large amounts of strain, making them ideal for ballistics testing applications [25]. Using a split Hopkinson bar setup, previous research conducted at NCSU has already shown that FBG's are capable of accurately measuring strain at strain rates up to 500 $s^{-1}$ [26]. At the speeds at which ballistic impacts occur, it is critical to have a sensing device capable of a high rate of data collection in order to avoid missing important facets of the test.

In addition to strain measurement, by placing the fiber directly behind the area of the fabric where the projectile will impact, it is possible to back calculate the maximum BFD of the impact [27]. However, despite their superior toughness when compared to metal foil gages, getting optical fibers with FBG's to survive the high stress environment induced upon it during impact remains a challenge and is the topic of this research.

Ballistics gelatin has proven to be the preferable backing material for FBG testing as it enables researchers to collect video footage of the BFD during impact, this is highly useful in determining the location of fiber failure during testing as well as for validating the deformation depths estimated [24]. Additionally, by imaging the fiber during impact, useful insights can be gained by matching the time domain of the strain data with the high-speed footage. Synthetic ballistics gelatin also has the advantage in that the testing block can be quickly readied for a second shot soon after the first, while the modeling clay currently used in the standard must be

heat conditioned to the correct stiffness and has to be remolded before each additional test. However, some testing involving modeling clay is still necessary as it is the specified backing material for standardized personal armor testing.

## 1.2 – Research Objectives

Objective 1: Investigate different materials and their suitability for spreading and dispersing the remaining kinetic energy behind a pad of soft body armor

Objective 2: Develop a robust sensing layer system capable of protecting embedded optical fibers during ballistic impact while minimizing the sensing layers overall effect on the BFD.

## 1.3 – Research Questions

Question 1: Which physical properties are ideal for the sensing layer to ensure the survivability of the FBG during and immediately following impact?

Question 2: How does the sensing layer material affect the maximum deformation due to impact as well as the deformation profile during impact?

## 1.4 – Thesis Outline

Chapter 1 gives an introduction to ballistic fabrics and the ongoing research into predicting soft body armor behavior during impact. Additionally, FBG strain sensing technology is introduced and discussed. Chapter 2 gives a detailed description of the test setup as well as the means by which data is collected and recorded as well as the backing materials and ballistic fabrics used. Chapter 3 discusses the material selection criterion used to select potential sensing layer materials and details the fabrication procedure for each sensing layer. Chapter 4 gives results from high speed testing of soft body armor pads with FBG embedded sensing layers. Strain data collected from the FBGs during impact as well as deformation data and fiber survivability are all

presented. Chapter 5 draws conclusions from the results given in the previous chapters and discusses future work which needs to be performed.

# CHAPTER 2 – Experimental Methods

The gas gun fixture in the Ballistics Loading and Structural Testing (BLAST) Lab at North Carolina State University was used to perform high speed testing on multi-layer Kevlar® KM2 soft body armor pads. A swept laser source was used in conjunction with an oscilloscope, high speed cameras, and 3D shape scanners to record strain and deformation values.

## 2.1 – Gas Gun Setup

In order to simulate the ballistic impact due to a firearm safely in a laboratory environment, a stationary gas gun setup was used for all of the high velocity testing described in this work. High pressure helium gas was used in the place of gunpowder to provide the driving force needed to accelerate the projectile. Figure 5 displays the gas gun used at NCSU and highlights each different component.

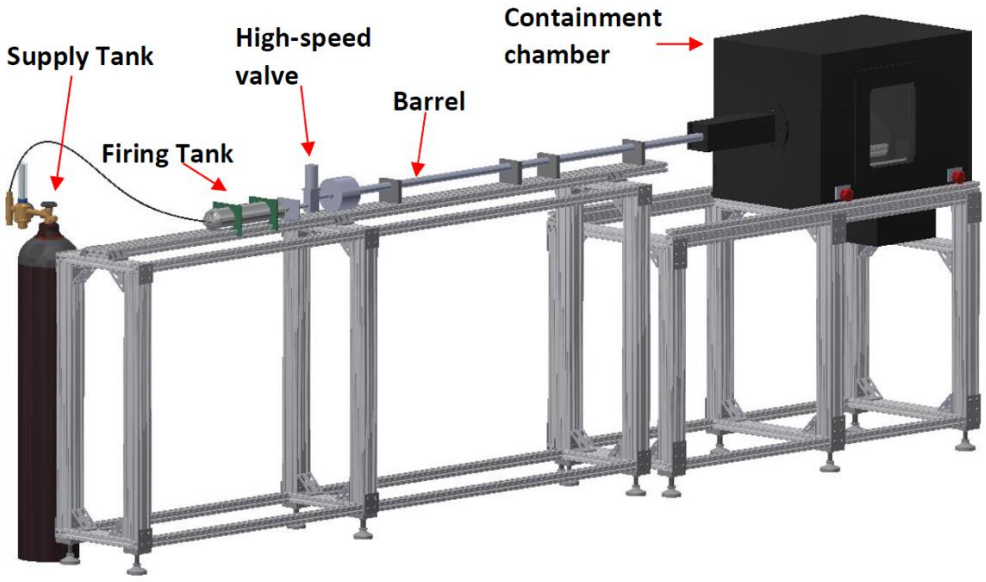


**Figure 5:** High Speed Gas Gun Setup [24].

The barrel used featured a 12.7 mm (0.5 inch) diameter smooth-bore hole with a length of 2 meters. The projectile is loaded into the barrel from a hole near the base, the hole then gets

plugged with a matching insert and the insert is held in place by the sliding locking sleeve. The gas gun has a maximum projectile size of 50 Caliber (0.5-inch projectile diameter). Early testing used a 0.5 inch steel ball bearing as the projectile [24] since it could be easily loaded and recovered after each shot. To better simulate a real-life scenario, the testing discussed in this work uses a 9mm (0.354 inches) copper plated lead projectile, 8.035 grams in mass, shown in Figure 4 and Figure 6. In order to allow a smaller diameter projectile to be fired down the barrel of the gas gun without a significant loss in velocity, it is necessary to mount the projectile in a sabot. The sabot (pictured in Figure 6) serves to widen the effective diameter of the projectile to 0.5 inches in order to allow sufficient pressure to build up behind the projectile during firing.

**Figure 6:** (Left) 9mm Sabot and (Right) Sabot with Mounted 9mm Projectile.

The sabots used are designed to have the arms peel away from the projectile during flight in order to prevent the added mass of the sabot from affecting the final results of the testing. The design has proven to be effective as shown in the still frames in Figure 7, The arms of the sabot separate mid-flight as intended but still have enough velocity to impact the target along with the projectile. While the arms of the sabot separate from the projectile, the base of the sabot remains with the round during impact. Therefore, the mass of the sabot's base (0.279 g) must still be considered when calculating the projectile's kinetic energy.

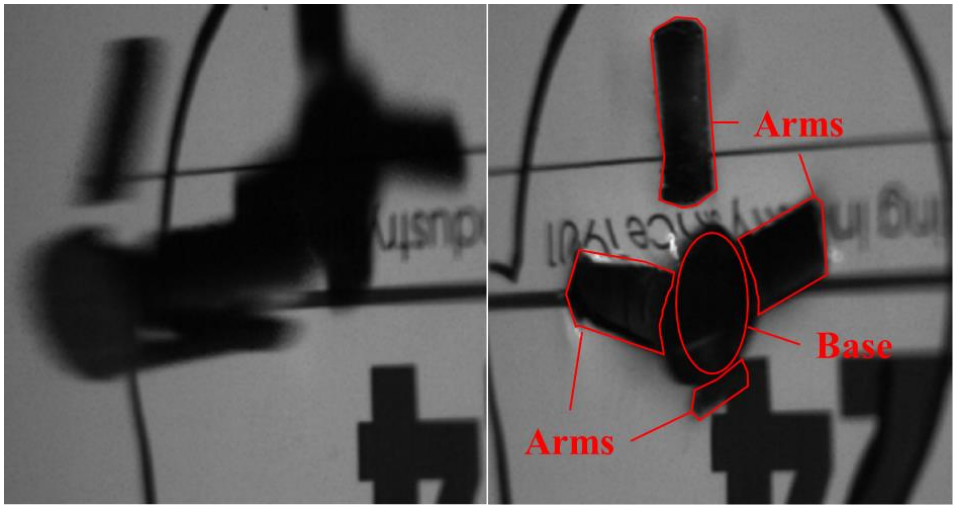


**Figure 7:** (Left) Sabot in Mid-Flight and (Right) Sabot 0.05 ms After Impact.

After the sabot and projectile have been inserted into the barrel and locked into place, helium can then be loaded into the firing tank pictured in Figure 5. Helium is introduced into the tank through the use of a pressure regulator valve. Should it be necessary, a release valve can be used to bleed excess helium. Once the desired pressure has been reached, the shot is performed by quickly dumping the helium into the barrel using a high-speed solenoid valve. The projectile then accelerates down the length of the barrel and exits into the containment chamber. Using a 6000 PSI tank of helium, projectile speeds of up to 456 meters per second have been achieved.

Once in the test chamber, the projectile impacts the Kevlar® shoot pack attached to the front of the mounted backing material block, as shown in Figure 8. A high intensity LED provides illumination for any testing involving high speed cameras and in the event of total perforation of the shoot pack and backing material block, a deflector plate is in place to guide the projectile safely into the catch basin.

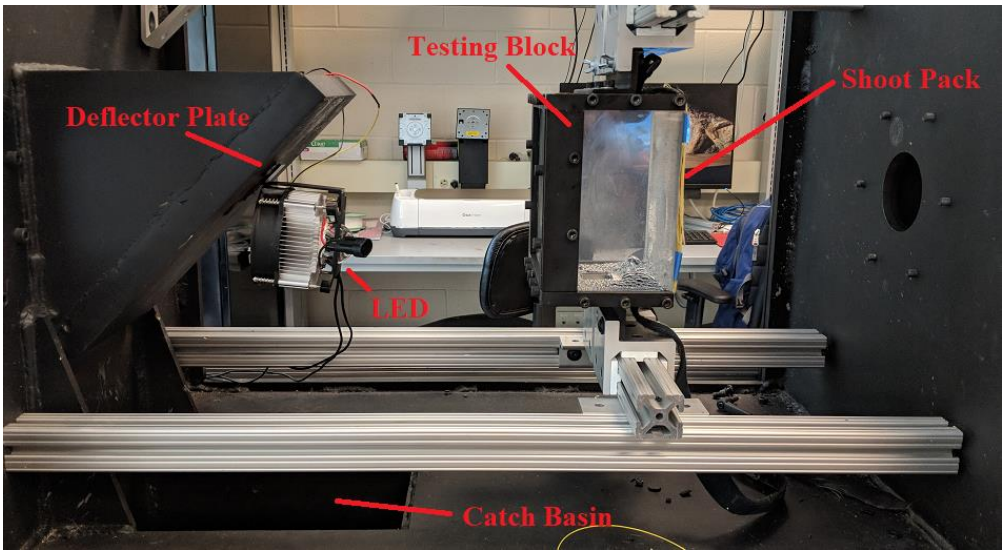


**Figure 8:** Containment Chamber Interior.

Note that while Figure 8 displays a block of ballistics gel, testing blocks using modeling clay as the backing material are mounted in the same manner.

## 2.2 – Shoot Packs and Backing Materials

Table 1 details the properties of the Kevlar® fabric used to create soft body armor pads (shoot packs) for testing. The Kevlar® was purchased as a roll from Barrday Inc. and was then cut and assembled into shoot packs at NCSU.

**Table 1:** Fabric Properties.

| **Fabric** | **Weave** | **Fabric Thickness (mm)** | **Denier** | **Breaking Strength (kN/m)** | |
|---|---|---|---|---|---|
| | | | | **Warp** | **Weft** |
| Kevlar® KM2® Plus | Plain | 0.17 | 500 | 87.6 | 96.3 |

Each shoot pack was roughly 16.5 cm (6.5 inches) square and consisted of multiple layers of Kevlar® ranging from 30-50 layers. Figure 9 depicts a prepared shoot pack from the top and side views.

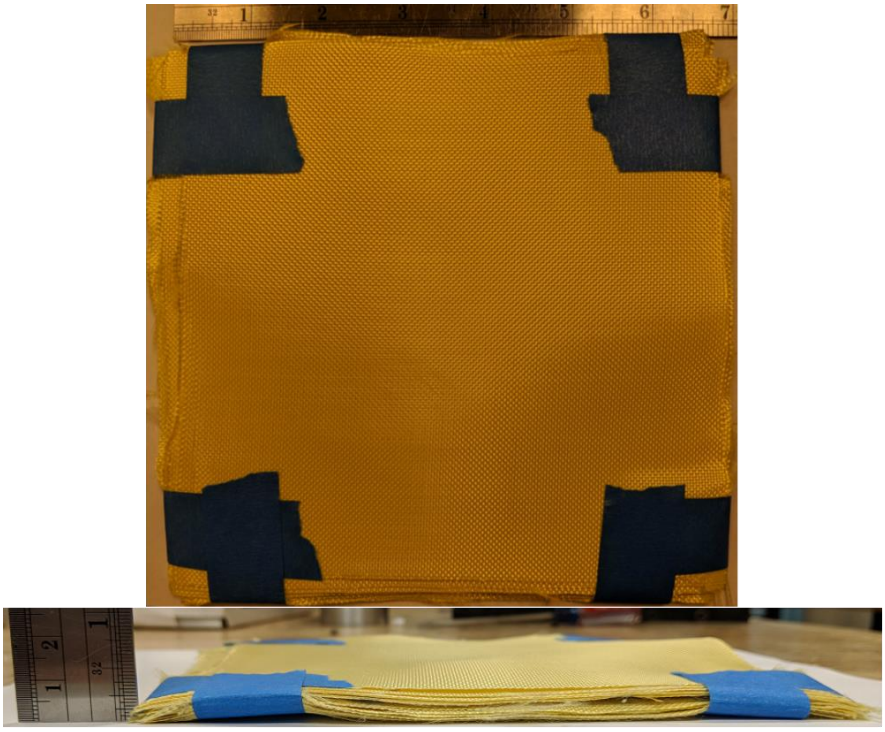

**Figure 9:** (Top) Top View and (Bottom) Side View of Shoot Pack.

Prior to testing, the shoot pack was loosely affixed to the backing material block by Velcro straps which run vertically across the edges of the pack. These straps serve to hold the shoot pack in place during impact without introducing any unwanted clamping boundary conditions.

Two different backing materials were used, Roma Plastilina #1 modeling clay and 20% NATO standard synthetic ballistics gelatin. The modeling clay was housed in a testing block 17.2x17.0 cm across and 10.2 cm deep. The ballistics gelatin block was 17.8 cm wide by 15.9 cm tall and 9.5 cm deep. Figure 10 displays the two different backing materials in their respective testing blocks.

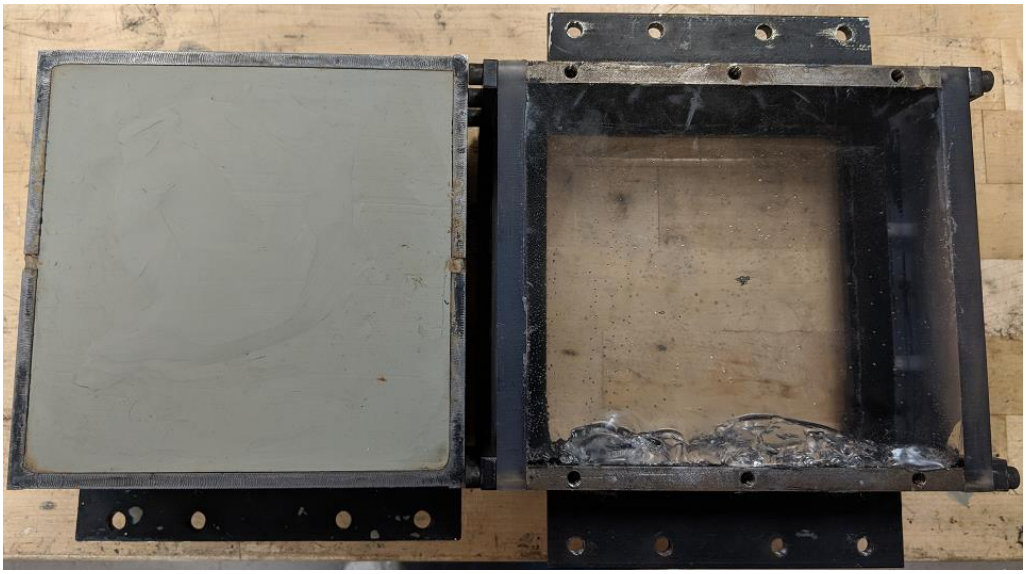

**Figure 10:** (Left) Roma Plastilina #1 Modeling Clay and (Right) 20% Ballistics Gelatin.

Recall that the modeling clay must be heated in an oven prior to testing in order to achieve the correct clay stiffness. Internal temperatures within the range of 85-95°$F$ are desirable for testing involving clay as a backing material [19]. For testing performed at NCSU, a Masterbuilt Electric Digital Smoker was used to heat the clay to the appropriate temperature.

The ballistics gelatin used was of the synthetic variety instead of the mixing powder alternative due to the fact that it could be melted and recast multiple times, improving its service life. The synthetic gelatin is also clearer than the powder variety, which is valuable when capturing camera footage during testing.

## 2.3 – Data Collection

Data collection during each high-speed impact test can be separated into three separate groups; data related to the projectile, data collected visually from high speed cameras or by 3D object scanners, and data collected from the FBG's.

### 2.3.1 – Projectile Data

The gas pressure used to fire the projectile is recorded immediately prior to each test. After firing, as the projectile approaches the end of the barrel, it trips two photogates, spaced 1 inch apart. An oscilloscope is set to begin recording once it measures the voltage from the first photogate dropping to zero. As the projectile continues down the barrel, it passes through the second photogate and the oscilloscope records the voltage drop from each photogate.

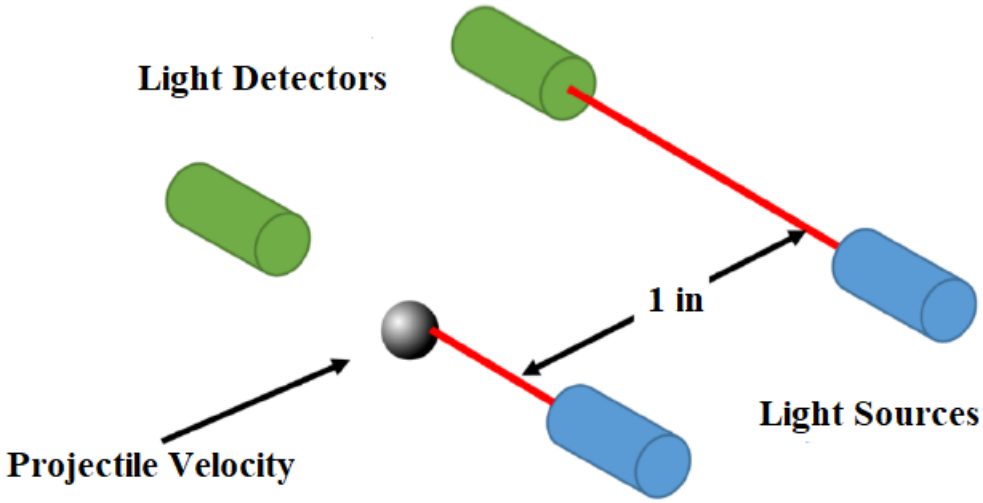


**Figure 11:** Photogate Diagram [24].

By measuring the time difference between the two voltage drops and since the distance between the two photogates is known, it is a simple matter to determine the velocity of the projectile as it is entering the containment chamber.

### 2.3.2 – Testing Block Data

For testing using modeling clay as a backing material, values for the temperature of the clay and the final BFD must be taken. Immediately prior to a test, the clay is removed from the oven and the temperature within the clay is measured in two separate locations using digital probe thermometers (shown in Figure 12).

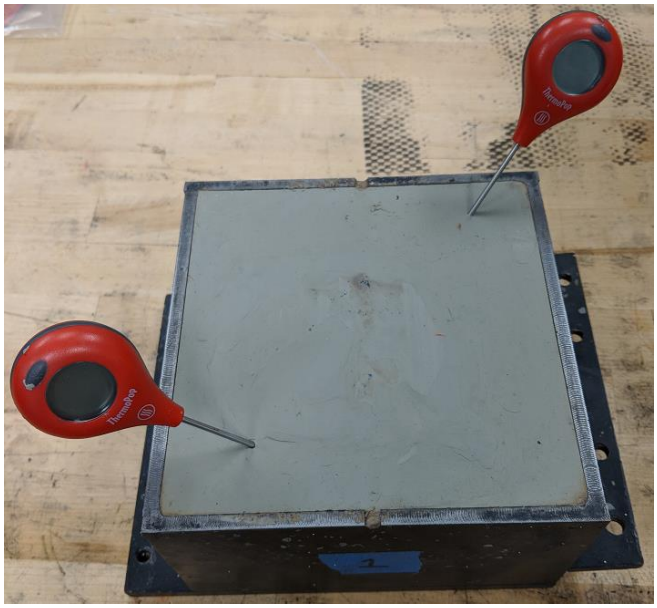

**Figure 12:** Thermometer Probe Locations for Clay Testing.

After the clay temperature has been measured, the block is mounted in the chamber and the test is performed. Once the test is complete, the testing block is removed from the containment chamber and the depth and diameter of the deformation are measured using a set of hand calipers as shown in Figure 13 below.

**Figure 13:** (Left) Deformation Width and (Right) Deformation Depth.

After hand measurements have been taken, a 3D scan of the testing block is generated using an iPad with an attached Occipital Structure 3D Scanner (see Figure 14).


**Figure 14:** Structure 3D Scanner [28].

Once all measurements have been taken, the deformation is filled back in and the clay block is smoothed over and placed back in the oven until the next test.

For tests involving ballistics gelatin, two Fastcam SA-X2 high speed cameras were set up and connected to the oscilloscope via BNC cables. The cameras and FBG devices were set to begin recording once they received a TTL trigger voltage from the oscilloscope. Figure 15 displays the order by which each system is triggered chronologically.

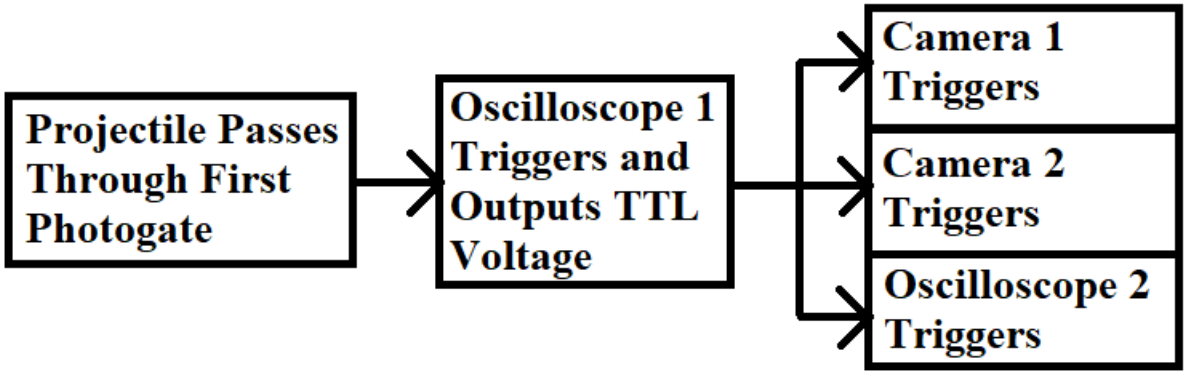


**Figure 15:** Trigger Diagram for Ballistics Gelatin Testing.

One camera was placed perpendicular to the testing block in order to capture deformation footage into the block. The second camera was placed so that it looked into the testing chamber from the back to view the shape of the deformation area. Figure 16 shows a top down view of the position of each camera in relation to the testing block.

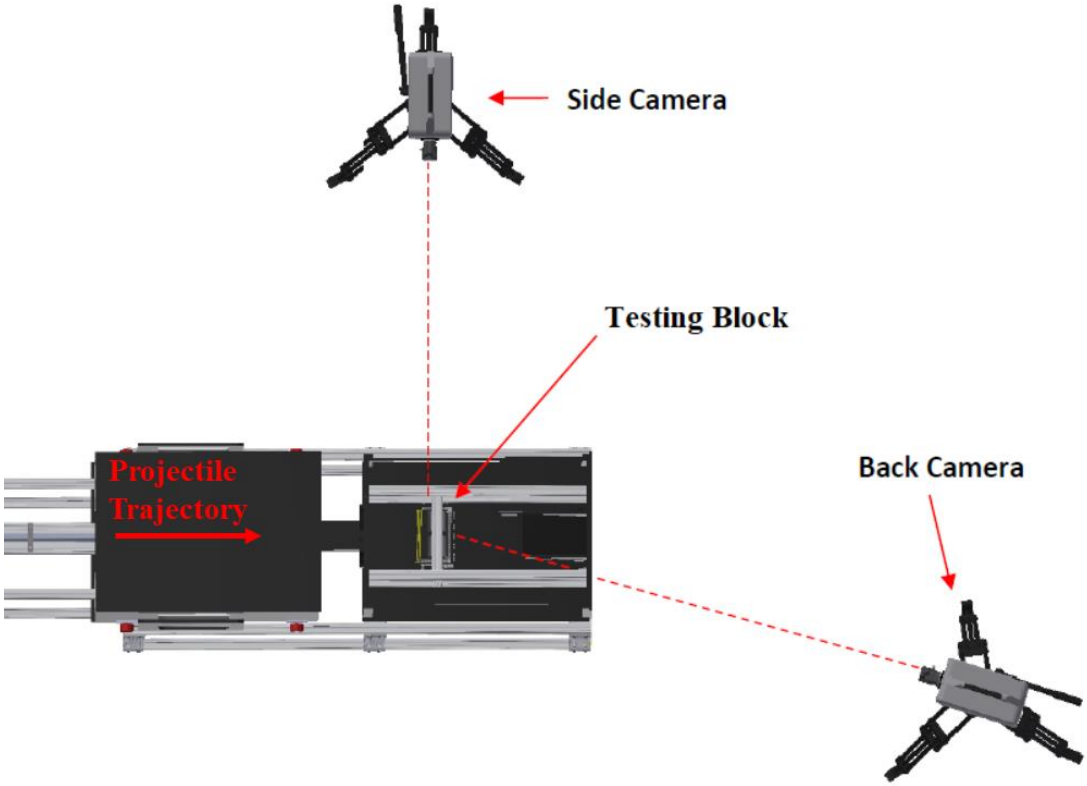


**Figure 16:** Top View of Camera Placement [24].

For all testing, the side facing camera was set to capture video at 100,000 frames per second with a resolution of 384x264 pixels. The back facing camera shoots video at 200,000 frames per second with a resolution of 256x152 pixels. Ideally, the back camera would be positioned directly behind the testing block but due to the need for a deflector plate, the viewing ports are offset from the center of the rear wall of the containment chamber.

### 2.3.3 – FBG Data

Strain measurement using optical fibers containing FBG's comprises the final portion of the data collection aspect of this work. In order to collect information regarding the reflected wavelength of the FBG, discussed in Section 1.1 above, an Insight High Swept Laser was used to collect the FBG output spectrum by sweeping through a light wave wavelength range at rates up to 100 kHz. Prior to the initiation of the test, the laser wavelength range is set according to the reflected wavelength of the FBG being tested. It is important to keep the wavelength range large enough so that the reflected wavelength of the FBG does not shift outside of the wavelength range of the laser during impact, as this would result in incomplete data being recorded. However, it is equally important to keep the range as narrow as possible as this will increase the sweep rate of the laser and generate a larger number of useful data points. The laser itself can also only output a finite range, this wavelength range extends from 1526 nanometers to 1605 nanometers. The FBG's must then be selected which have a reflected wavelength within the limitations of the laser.

During testing, swept light from the laser travels through insulated optical fibers into a circulator which directs the light into the fiber containing the FBG. The light then travels through the FBG at which point the reflected wavelength is bounced back down the fiber. The light then returns to the circulator where it reaches a photodiode. The photodiode converts the amplitude of the reflected light at each wavelength from the laser sweep into the waveform voltage data which is then recorded by Oscilloscope 2 (see Figure 15). In Figure 17, a diagram of the laser interrogator system is depicted to further illustrate the path the light takes through the equipment and FBG.

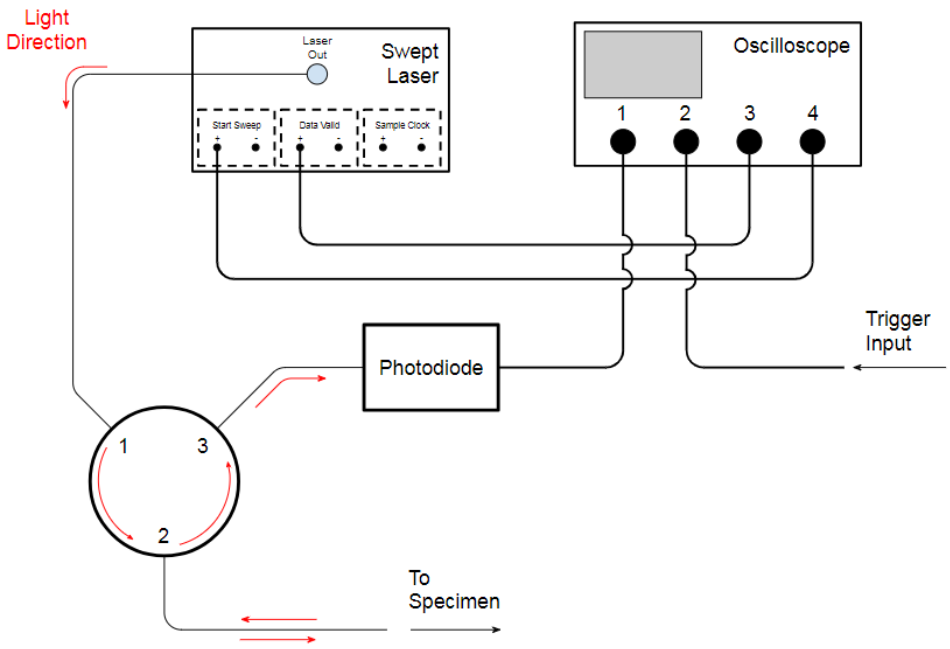


**Figure 17:** Swept Laser Setup.

Once the laser reaches the end of its wavelength range, it initiates another sweep and the process repeats itself. Along with the Waveform data produced by the photodiode, the laser also outputs start sweep and data valid values which get recorded by the oscilloscope during testing to help in the post processing phase. The start sweep data is simply a square wave which jumps up to the maximum value when the laser initiates a new sweep and falls to zero once the sweep ends. The data valid wave should appear to move between an upper and lower value. The upper data valid value gets output when the waveform data from the laser is valid and the lower value gets output when the waveform data point is invalid. The waveform, start sweep, and data valid files from the oscilloscope can then be saved as binary (.bin) files.

## 2.4 – Data Processing

Additional post processing was necessary in order to convert the raw data from the various devices discussed into useable information regarding the BFD and time dependent strain data.

### 2.4.1 – Clay Backing Material

For shots which utilized Roma Plastilina #1 modeling clay as the backing material, the final dimensions and volume of the deformed region were found using the scans generated by the structure scanner. The scanner created Object (.obj) files of the testing block which could then be converted into a Standard Tessellation Language (.stl) format as shown in Figure 18 and read into Solidworks or another CAD software as a solid body.

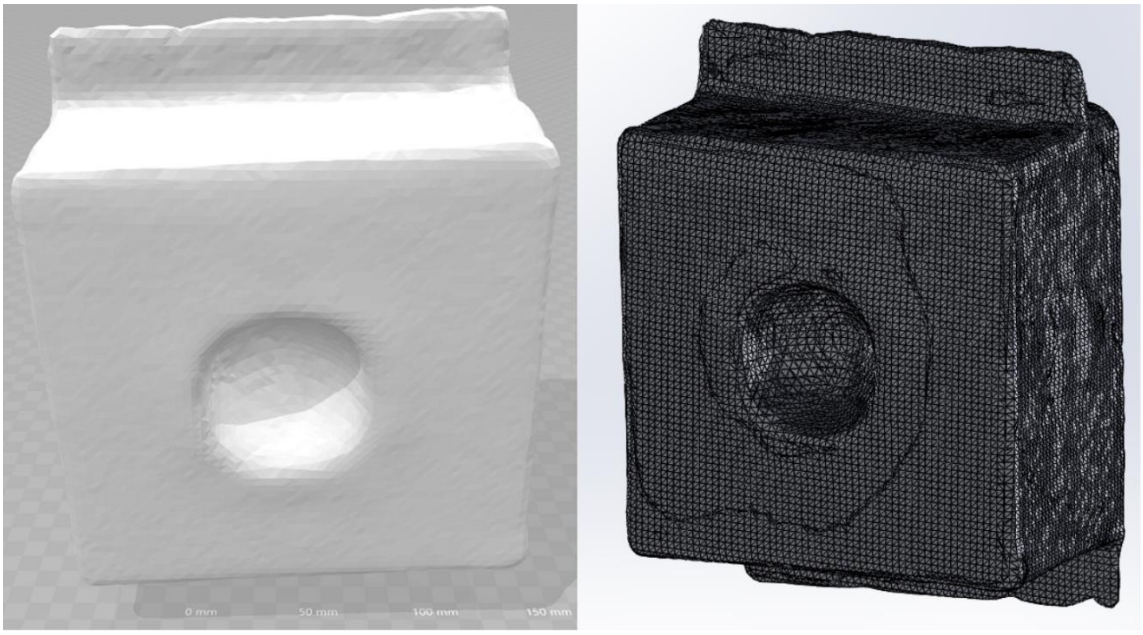


**Figure 18:** (Left) STL Model of Deformation and (Right) Solid Body of Deformation.

By then extruding a second body through the center of the deformation and performing a volume subtraction operation, it was possible to create a solid body object of the deformation hole, as shown in Figure 19.

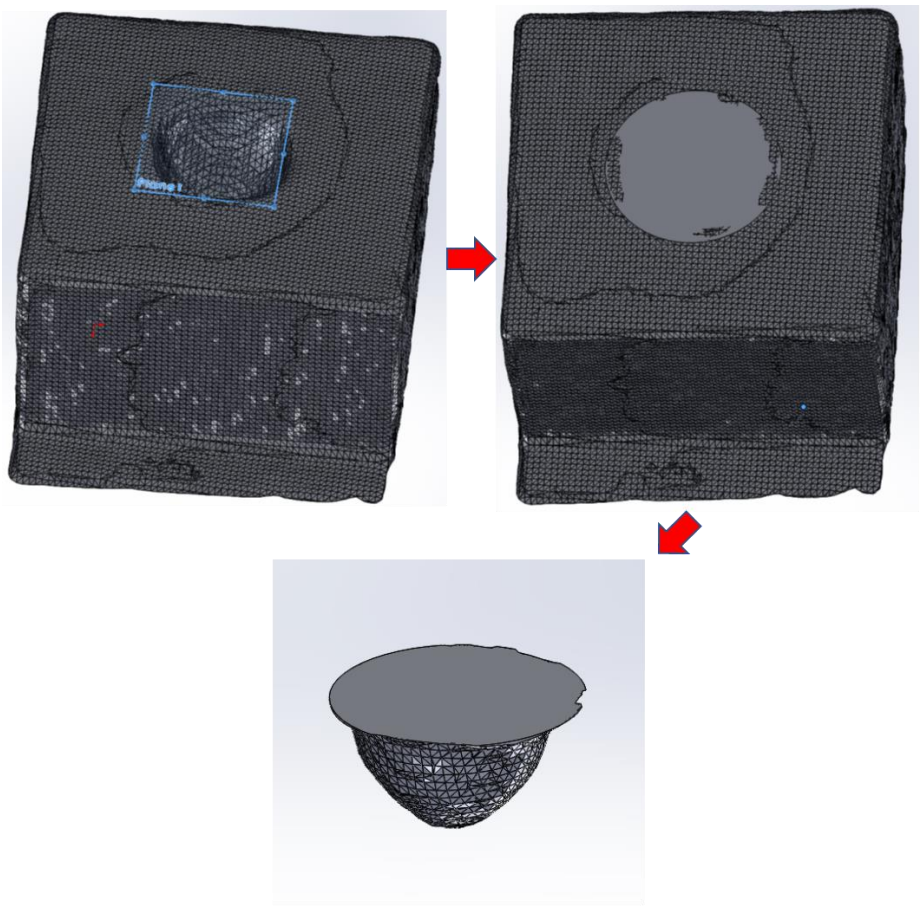

**Figure 19:** (Top Left) Model with Reference Plane, (Top Right) Extruded Body, (Bottom) Solid Body of Deformation Volume.

After the deformation shape in the clay had been backed out from the 3D scan, it was possible to take measurements in SolidWorks® of the deformation's physical dimensions, such as diameter, depth, and deformation volume. It should be noted that since the modeling clay is opaque, it is not possible to collect any data on the BFD during impact using visual methods. The FBG sensing array is then the only means to collect time dependent data when using clay as the backing material.

### 2.4.2 – Ballistics Gelatin Backing Material

In tests utilizing ballistics gelatin as the backing material, high-speed video was used to measure the BFD values as the impact progressed to maximum deformation. This was useful when attempting to validate any models which estimate the BFD using strain data gathered from the FBG sensor in place behind the shoot pack. For this purpose, an image processing script was written in MATLAB to take the raw footage from the camera and return depth versus time data [24]. Since the index of refraction of the ballistics gelatin is different than that of the surrounding air, as the deformation occurs, the surface of the gelatin in the deformation region will take on a silvery appearance as the light from the LED is reflected back towards the camera. Figure 20 illustrates the contrast between undeformed gelatin and the surface of the gelatin in the deformation area.

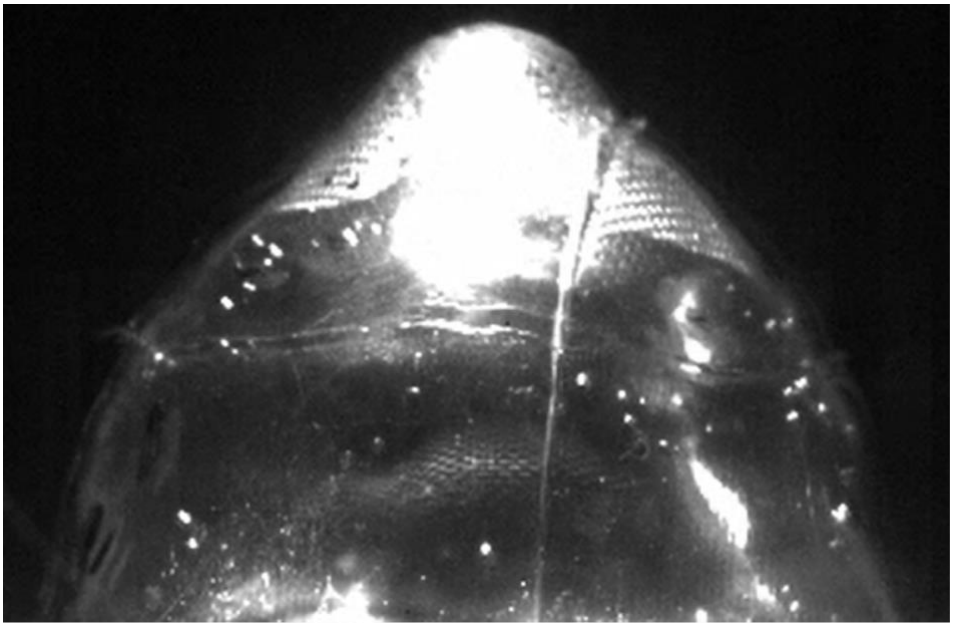

**Figure 20:** BFD Contrast Within Ballistics Gelatin.

The image processing script takes advantage of the high amount of contrast between the impact region and the undeformed gelatin shown in Figure 20 and converts the raw grayscale

footage into black and white video. By adjusting the threshold at which a grey pixel is considered bright enough to be turned into a white pixel, the code can take advantage of the bright impact region to turn the entire deformation profile into white pixels, while the remaining area is converted into black pixels. Figure 21 demonstrates the conversion of a grayscale deformation profile into a black and white deformation profile.

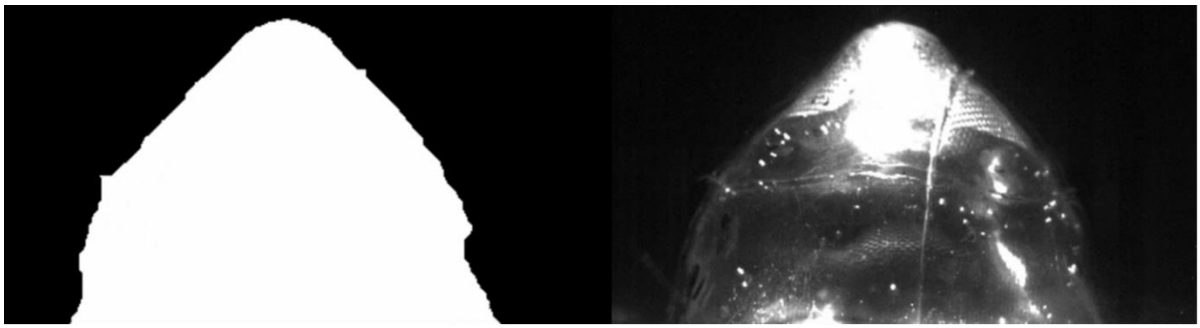

**Figure 21:** (Left) Black and White Conversion of (Right) Greyscale Deformation Image.

As seen in Figure 21, the image processing script is able to accurately convert the deformation profile into a black and white format, from which data regarding the deformation dimensions can be extracted [24]. In order to convert pixel values into useful length data, 12.7 mm (0.5 inch) and 25.4 mm (1.0 inch) calibration rods were pressed into the gelatin to give a reference point when converting the data [24]. Figure 22 gives examples of calibration snapshots taken during ballistics gelatin testing

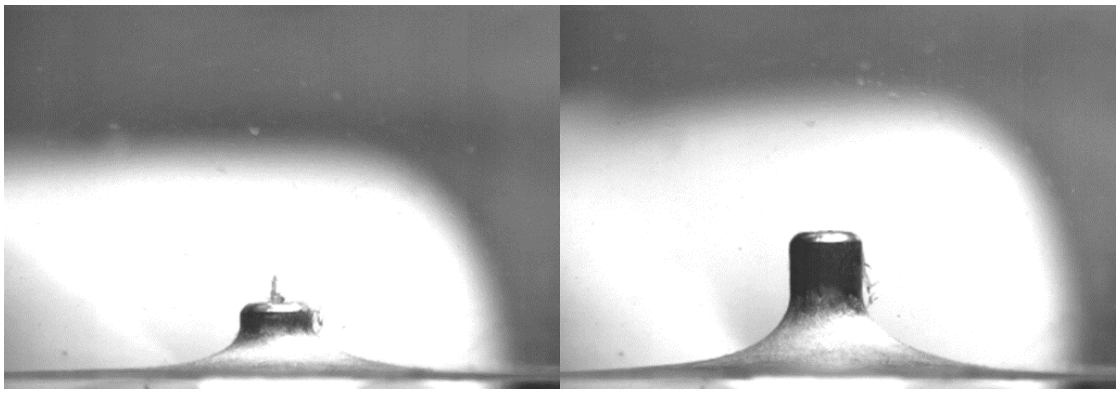

**Figure 22:** (Left) 0.5 Inch Calibration and (Right) 1.0 Inch Calibration Snapshot.

Using the calibration snapshots, a pixel to inch conversion factor, $C$, can be determined using Equation 1 below.

$$C = \frac{1}{2(H_{1.0} - H_{0.5})} \quad (1)$$

Where, $H_{1.0}$ is the pixel row index for the 1.0 inch calibration rod and $H_{0.5}$ is the row index of the 0.5 inch calibration rod [24]. It is important to note that the calibration snapshots are only accurate if the cameras remain in position following calibration and are not moved.

Inconsistencies in the gel such as small bubbles or debris suspended in the gelatin can cause bright spots outside of the deformation which may distort the profile during black and white conversion. It is possible to delete small patches of white pixels from the final video but it is still important to create a testing block which is as clear as possible to avoid any errors.

### 2.4.3 – FBG Sensor Data

To generate useful information regarding the strain behind the armor system, the data collected from the FBG was put through several processing steps. The FBG operates by reflecting a narrowband wavelength of light back towards the laser source. Each grating has a periodic variation in the refractive index (see Figure 23) of the fiber core in order to create a focused reflected peak.

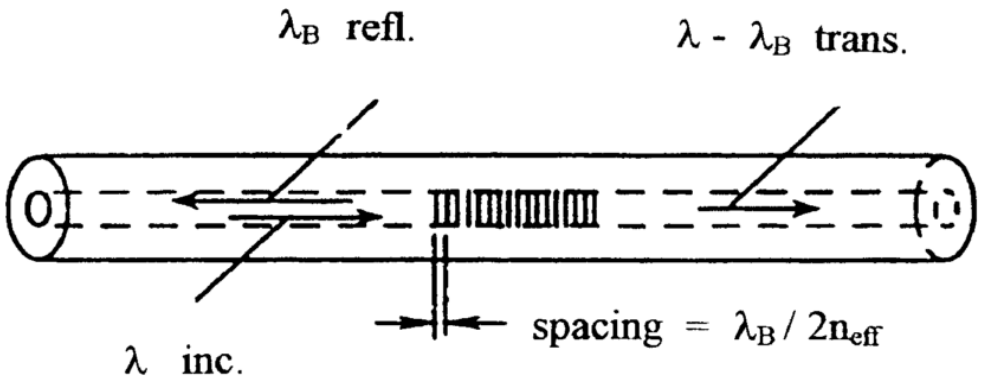


**Figure 23:** Diagram of Fiber Bragg Grating [29].

As the optical fiber is strained, the wavelength which the FBG reflects will shift to higher and lower wavelengths depending on whether or not the FBG is in tension or compression. The amount that the wavelength shifts has been shown to be proportional to the strain experienced by the FBG as well as the change in temperature seen, as shown in Equation 2 [25].

$$\frac{\Delta\lambda}{\lambda_0} = k\varepsilon + \alpha_\delta \Delta T \tag{2}$$

Where $\Delta\lambda$ is the shift in wavelength, $\lambda_0$ is the initial wavelength at the start of the test, $k$ is the strain gage factor, $\varepsilon$ is the strain, $\alpha_\delta$ is the temperature gage factor and $\Delta T$ is the temperature change. By holding the temperature constant during the test, Equation 2 can be simplified to show:

$$\varepsilon_m = \frac{\Delta\lambda}{k\lambda_0} \tag{3}$$

Where $\varepsilon_m$ is strain due to mechanical effects. Taking the waveform data collected using the swept laser setup detailed in Section 2.3.3 above, Equation 3 can then be used as a means to measure strain.

To accomplish this, the .bin files from each test were read into a MATLAB script generated by Fredrick Seng, a researcher at Brigham Young University. The script uses the data valid and start sweep files from the oscilloscope to split the waveform data up into the individual spectra from each laser sweep and delete any invalid data points. The new waveform data then gets stored into a matrix in which each row contains the waveform voltage values of a single sweep [26]. By locating the maximum voltage of each spectrum, the maximum reflected wavelength of the FBG can be found. Then, by determining the difference in reflected wavelength from one spectrum to the next, the strain value within the FBG can be found using Equation 3. Using this method, strain data for the entire impact can be recorded, assuming the

fiber containing the FBG survives throughout the test. Figure 24 gives an example of the spectrum data generated from a typical ballistic impact test with an FBG sensor.

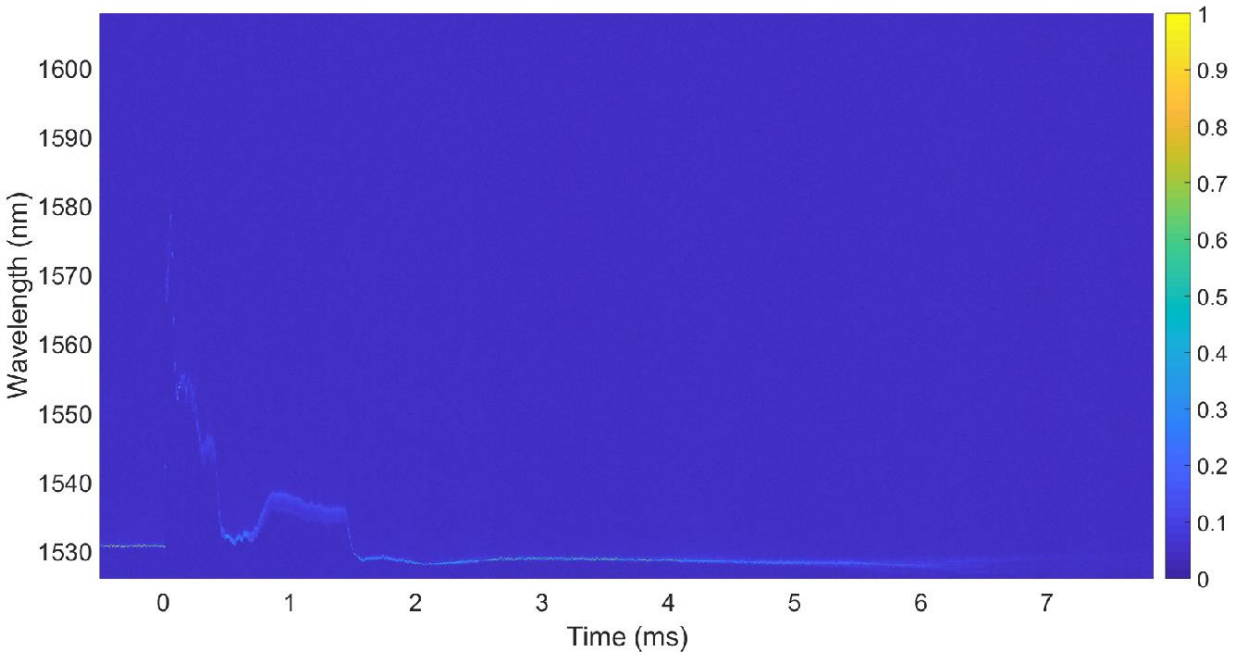


**Figure 24:** Example Wavelength Data.

The graph above was generated using the waveform data collected from the photodiode. The vertical direction of the figure represents the wavelength sweep range of the laser. Reflected light from the FBG registers as a higher voltage than the remaining sweep range. By tracking the peak voltage of each laser sweep, it is possible to record the wavelength shift of the FBG during impact.

## 2.5 – Summary

The experimental setup for high speed projectile impact testing at NCSU was described. 9 mm FMJ bullets were used as the projectile with plain woven Kevlar® KM2® Plus serving as the body armor fabric. Two backing materials were selected, 20% NATO standard ballistics gelatin and Roma Plastilina #1 modeling clay. For each backing material, the techniques for gathering

data on the projectile, deformation dimensions, and the FBG waveform were detailed. The ballistics gelatin backing material utilized high speed cameras positioned at the back and sides of the testing chamber to measure the deformation. For tests using modeling clay, the final deformation dimensions were measured by hand and the deformation profile was obtained through the use of a 3D structure scanner. In the following chapter, methods for mounting the FBG to the testing block are discussed. In particular, the different materials utilized in the sensing layer are reviewed as well as the means by which the FBG was attached.

# CHAPTER 3 – Sensing Layer Material Selection

This chapter discusses the different sensing layer materials which were studied and how the final material was selected from the candidates. The criterion used to select each material is discussed and the methods used for fabricating each sensing layers are given.

## 3.1 – Sensing Layer Selection Criterion

Although the soft body armor pad used in testing greatly reduces and disperses the high kinetic energy of the projectile upon impact, there is still a significant amount of energy transferred to the region of the backing material directly behind the impact and in the surrounding area. The residual energy behind the shoot pack combined with the fact that the testing discussed often goes well past the established 44mm criterion covered in section 1.1 means that the sensing layer is subject to a hostile testing environment.

An adequate sensing layer must then be able to protect the fiber from the energy present behind the shoot pack during impact so as to prevent the FBG from fracturing. Since the majority of the useful data for each test is collected immediately following impact and as maximum deformation is reached, it is critically important that the fiber be able to survive through the initial impact, when the forces on the fiber are highest. However, it is also important that the sensing layer does not influence the back-face deformation of the soft body armor. Using a material that is too stiff or thick would reduce the amount of BFD seen during impact and could lead to inaccurate testing data.

The sensing layer must also be able to freely move with the soft body armor pad during impact and therefore should be highly pliant with a large strain to failure value, similar to the Kevlar®. In addition to the mechanical properties of the sensing layer, it is also important that

the FBG can be easily mounted or embedded within the sensing layer without introducing any unwanted boundary conditions which may affect the test results.

## 3.2 – Kevlar® Based Sensing Layers

Initially, Kevlar® KM2® Plus squares from the same cloth roll as the fabric detailed in Table 1 were used as the sensing layer onto which the FBG optical fibers were attached. It was reasoned that because Kevlar® was known to have a high strain to failure rate and since the plain-woven fabric had good drapability, a Kevlar® sensing layer would be a good candidate. Since the sensing layer and shoot packs were of the same material, it also proved convenient when preparing test samples. Each sensing layer was cut to be approximately 165x165 mm (6.5x6.5 inches) in order to match the dimensions of the shoot packs.

One challenge faced with using Kevlar® as the sensing layer material was how to attach the FBG's to the sensing layer. Due to the mechanical properties of the optical fibers, FBG sensors are robust when loaded in compression transversely or in tension linearly along the fiber length but perform poorly when subjected to shear or bending stresses. The fiber then needed to be attached in a way which minimized bending and shear stresses placed on the fiber while still holding the fiber securely enough to prevent lateral movement of the fiber away from the impact center. Initially, the fiber was woven into the sensing layer itself, as shown in Figure 25 below.

**Figure 25:** Kevlar® Sensing Layer with Woven Fiber.

The fiber was woven into the sensing layer by using a sharply pointed object to loosen individual yarns along the desired path of the fiber. The fiber was then inserted underneath the

loosened yarns while remaining above the rest of the fabric. While it was easy to attach the fiber to the sensing layer in this way, the method was discarded once it was observed that the yarns did not allow the fiber to slip easily as it was loaded which resulted in larger amounts of stress being placed on the fiber. Due to this, the majority of the woven fibers tested broke during impact.

Instead of weaving the fiber into the Kevlar® itself, loose stitches were used to attach the fiber to the surface of the sensing layer. In this way, it was possible to keep the fiber flush against the surface of the fabric without introducing any crimping along the length. The stitches also served to prevent lateral movement away from the center of deformation while still allowing the fiber to slide inward while the impact progressed. Figure 26 shows an FBG mounted onto a Kevlar® sensing layer with fabric stitches.

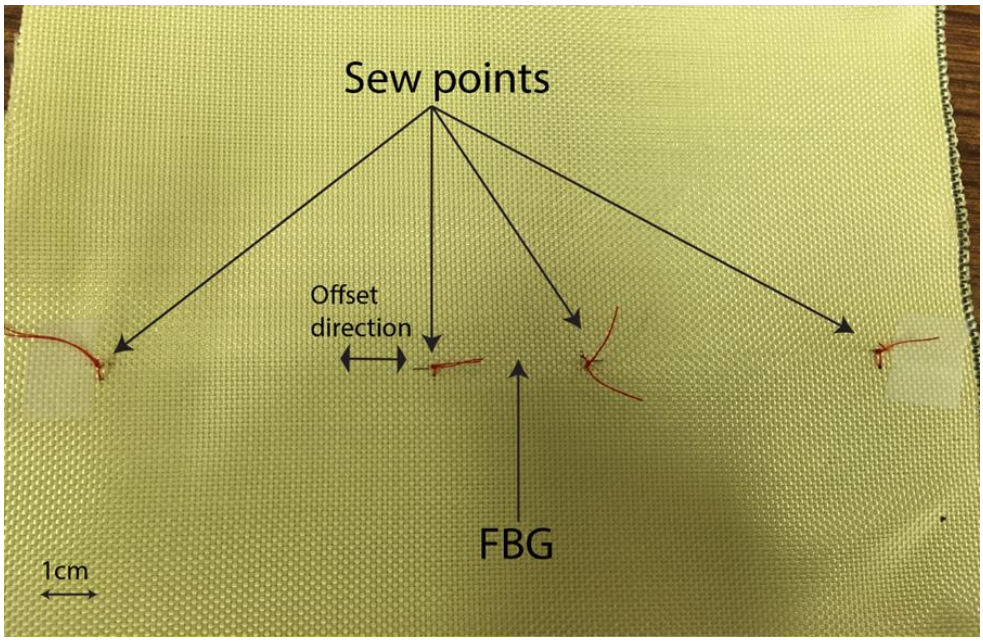


**Figure 26:** Kevlar® Sensing Layer with Stitched Fiber.

The image shown in Figure 26 is of a loosely stitched FBG. By only loosely tying the stitches, it reduced the amount of shear stress present on the fiber at the stitch locations. Each

stitch is a single loop of fabric. The two center stitches are separated by 3 cm and the outside stitches are separated by 5 cm. If the stitches on the fiber are too tight, there is risk of damaging the fiber during stitching and the amount of stress on the fiber increases as it is more tightly constrained. Stitch location in relation to the impact area also proved to be important as stitches placed too far apart resulted in the fiber moving laterally away from the center of the impact. As the impact progressed, samples with the stitch locations too far apart would experience the fiber slipping down the side of the deformation as there was no restraining force acting to keep it on the center of the cone. This lateral slipping also resulted in unwanted shear and lateral forces acting on the fiber which distorted the FBG results. Conversely, stitches placed too close together are also undesirable. Due to the large compressive force seen near the impact center, stitches in this region can tighten against the fiber and cause it to bind at the stitch location. As the center of the impact continues to elongate, the fiber is quickly stretched past its maximum allowable strain if not allowed to slip freely. Once the fiber has bound against a stitch, it is also subject to added shear stress as the impact zone reaches the stitch location and pulls the fiber into a tight radius against the stitch.

## 3.3 – Silicone Based Sensing Layers

As an alternative to sensing layers made from Kevlar®, silicone was selected as a potential candidate due to its high strain to failure and elasticity. Silicone was also desirable due to the fact that it was in a liquid state initially and could therefore be cast around the fibers in order to create a sensing layer with a fully embedded FBG sensor. Two different types of platinum-cure silicone rubbers, Smooth-Sil 950 and Sorta-Clear 40 were chosen due to their good tear strength and abrasion resistance, as well as their low elastic modulus and high strain to failure values. Table 2 gives the technical data for each material.

**Table 2:** Silicone Properties.

| | **Smooth-Sil 950** | **Sorta-Clear 40** |
|---|---|---|
| **Mix Ratio by Weight** | 100A:10B | 100A:10B |
| **Pot Life (hrs)** | 0.75 | 1 |
| **Cure Time (hrs)** | 18 | 16 |
| **Specific Volume ($\frac{mm^3}{g}$)** | 805.6 | 924.9 |
| **Shore Hardness** | 50A | 40A |
| **Tensile Strength (MPa)** | 5.0 | 5.5 |
| **100% Modulus (MPa)** | 1.9 | 0.6 |
| **Elongation at Break (%)** | 320 | 400 |
| **Die B Tear Strength ($\frac{KN}{m}$)** | 27.1 | 21.0 |

The Smooth-Sil 950 silicone is a pale blue in color and is completely opaque while the Sorta-Clear 40 has a similar transparency to water. Figure 23 shows example sensing layers of both the silicone variations.

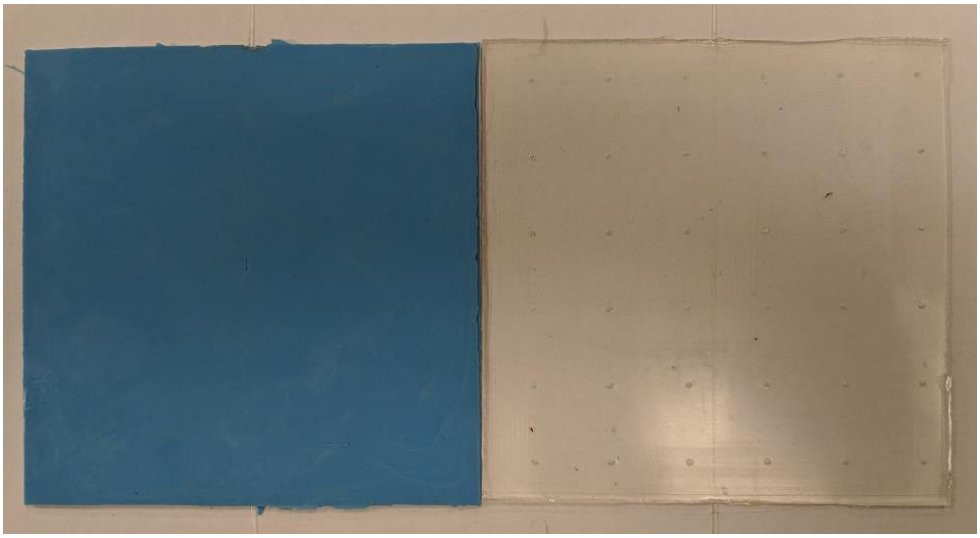

**Figure 27:** Example Sensing Layers of (Left) Smooth-Sil 950 and (Right) Sorta-Clear 40.

From Table 2, it can be seen that both silicone types have similar pot life and cure times. The Smooth-Sil has a greater resistance to tearing than the Sorta-Clear which helps in preventing the sensing layer from perforating during impact. However, the Sorta-Clear's 100% Modulus, or

the force exerted at 100% elongation, is significantly lower than the Smooth-Sil, indicating that it would flex and stretch more easily during impact. Picking one silicone type over the other based purely on the mechanical properties proved difficult. The Smooth-Sil 950 was more resistant to tearing during testing, however, Sorta-Clear 40 was softer and more elastic which is useful in directing residual energy away from the fiber. Due to the difficulty in selecting one type of silicone over the other, both variations were tested using the gas gun set up at NCSU in order to make a final material selection.

## 3.4 – Silicone Fabrication

To fabricate cast silicone samples, molds in the desired shape had to first be created. Using a laser cutter machine, 5.556 mm (7/32 inches) thick, smooth acrylic sheets, square panels 15x15 cm in size were cut to form the bottom and top of each mold. The top piece of the mold was then perforated with small holes through the thickness so that trapped air within the silicone had a pathway to escape during curing. 1.5875 mm (1/16 inches) thick acrylic was then cut into the shape of the mold cavity (see Figure 28).

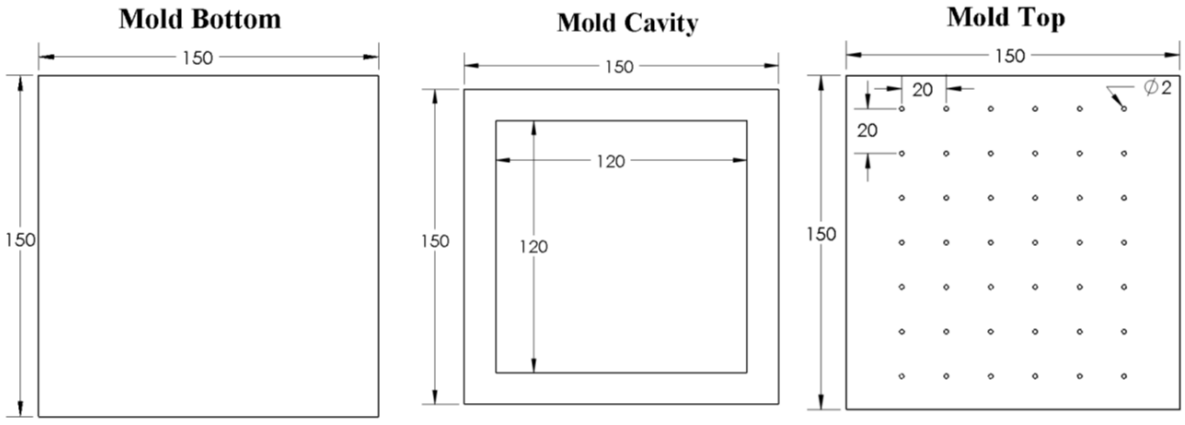


**Figure 28:** Mold Drawings (mm).

After the mold cavity had been fabricated, the laser cutter was used again at a lower power setting to engrave a small groove in the sides of the cavity. The groove served to keep the

fiber aligned through the center of the mold during the curing process. In order to prevent the fiber from slipping through the grooves and sagging to the bottom of the mold, modeling clay was pressed on top of fiber at each end of the mold to hold it in place and ensure that it remained taut as the silicone cured. The molds assembled produce samples approximately 2 mm in thickness. Later on, an aluminum insert 0.8128 mm (0.032 inches) thick replaced the original acrylic mold cavity in order to reduce the total thickness of the mold to approximately 1 mm. Figure 29 shows fully assembled molds for both 1 mm and 2 mm samples.

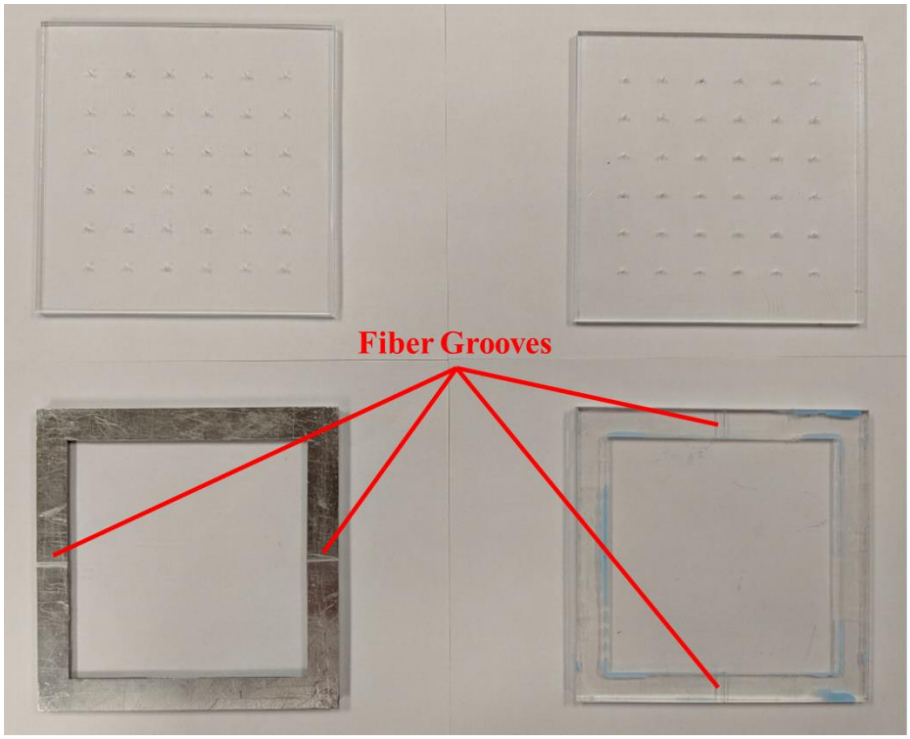


**Figure 29:** (Left) 1 mm Mold and (Right) 2 mm Mold.

The silicone was then measured out into a mixing cup using a digital scale to achieve a 10:1 ratio of part A to part B. For the 2 mm thick samples produced, roughly 60 grams of part A and 6 grams of part B was used. For the 1 mm thick samples, 30 grams of part A and 3 grams of part B were used. After both parts had been measured out into the cup, they were thoroughly mixed together in order to achieve a high degree of cross linking between the two parts and

avoid any uncured spots in the final product. Although mixing is a necessary step in the fabrication process, it introduces a large quantity of air into the silicone mixture, as shown in Figure 30.

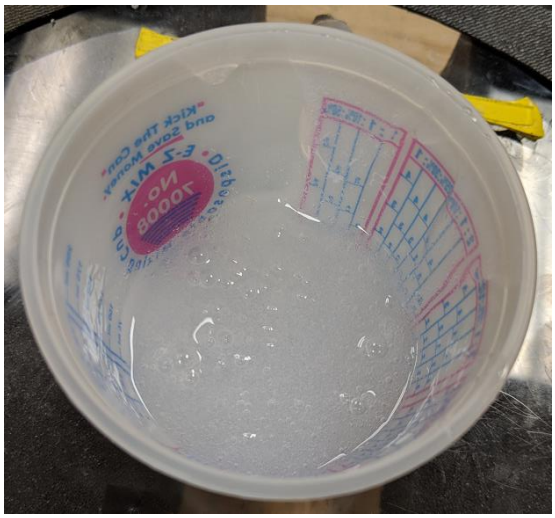

**Figure 30:** Freshly Mixed Sorta-Clear.

Depending on the viscosity of the silicone used, this air may not escape entirely if cured at atmospheric pressure. Sensing layers created with a large amount of trapped air will negatively affect the performance of the sensing layer during testing by reducing the overall amount of silicone present within the sensing layer. Figure 31 demonstrates a Sorta-Clear sample with entrapped air underneath the surface of the sample.

**Figure 31:** Sorta-Clear Sample With Large Amount of Trapped Air.

From the figure above, it is clear that the trapped air pockets serve to reduce the overall cross-sectional area of the sample. Additionally, the bubbles act as stress concentrations which greatly lower the tear strength of the sample.

In order to create fully dense samples, it was necessary to degas the silicone immediately after mixing and before it had reached its pot life, at which time the silicone became too viscous for trapped air to escape. For this purpose, a custom vacuum chamber was created at NCSU. The vacuum chamber used a glass dome sealed to a polycarbonate base underneath onto which a vacuum inlet and release valve were attached. An image of the vacuum chamber is given below in Figure 32.


**Figure 32:** NCSU Vacuum Chamber Setup.

The silicone was then degassed in its mixing cup for approximately 15 minutes at a gage pressure of -25 in-hg. After the initial degassing period, the silicone mixture was poured into the mold and degassed without the lid for an additional 20-30 minutes, depending on the type of silicone used. Once degassing was completed, the mold was removed from the vacuum chamber and the top portion was placed over the mold cavity. Weights were then placed on top of the mold in order to ensure a good seal between the top and bottom portions. The silicone was then allowed to fully cure. Figure 33 shows two Sorta-Clear samples immediately after being covered and weighted.

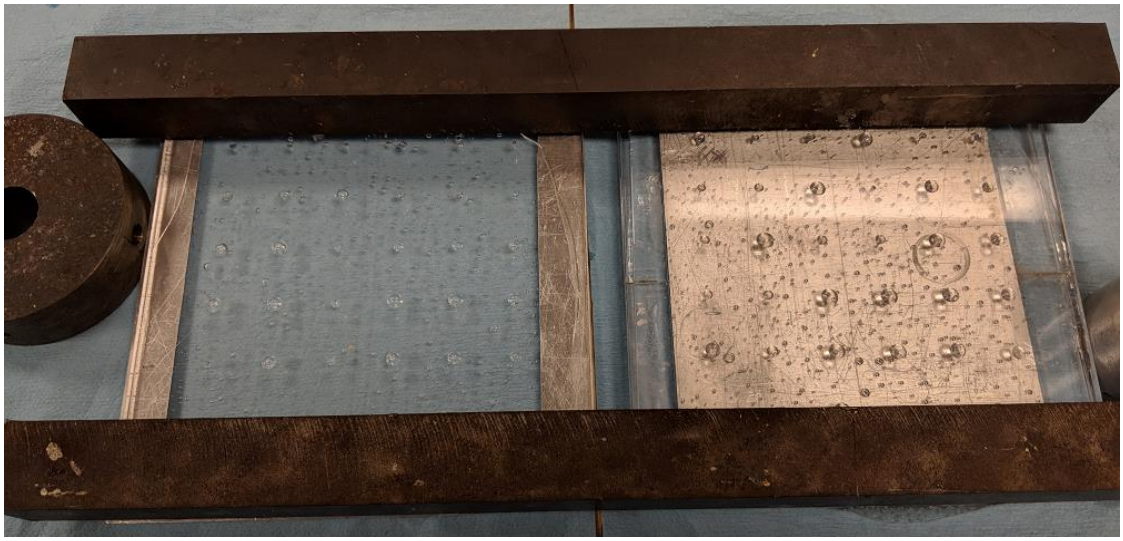

**Figure 33:** Sorta-Clear Samples Immediately After Degassing.

It can be seen that the silicone contains some entrapped air following degassing. The remaining air is able to escape out through the perforations on the top half of the mold as the silicone fully sets. Excess silicone can also flow out through the perforations after the lid has been placed which facilitates an even layer of silicone.

After the silicone had fully cured, the excess silicone was trimmed off the top of the lid and the lid was carefully removed by using a flat headed instrument to separate the top and bottom portions of the mold. After removal, excess silicone still remains around the edges and on the surface of the samples, as shown in Figure 34. Using a sharp blade, the excess material was removed from the sample.

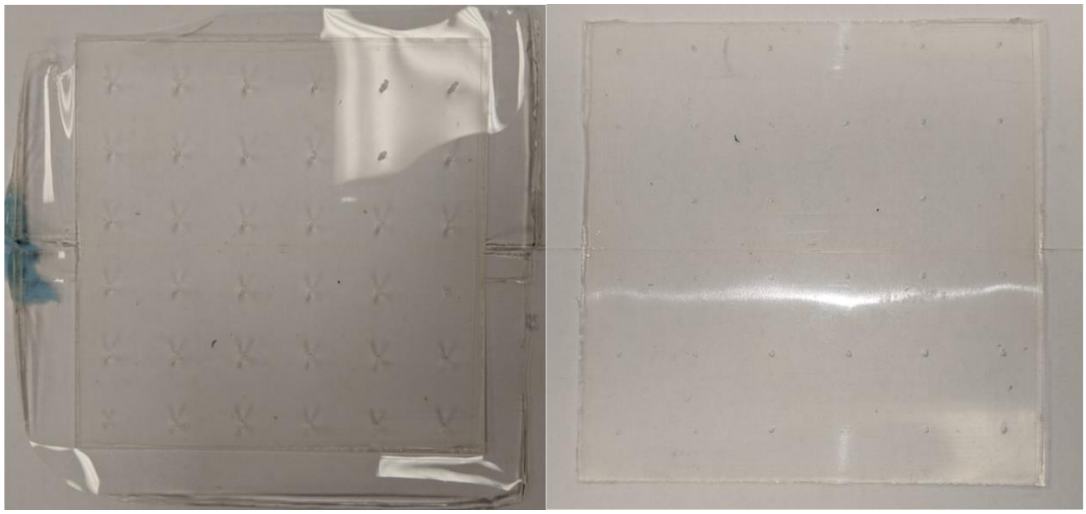

**Figure 34:** (Left) Untrimmed and (Right) Fully Prepared Sorta-Clear Sample.

Despite degassing all samples, some still contained small bubbles following curing. Sensing layers which contained only a small number of bubbles were deemed acceptable so long as they did not intercept with the fiber. Too many bubbles present along the length of the fiber may affect the strain measured by the sensor as it changes the friction interaction between the fiber and the silicone. Bubbles near the fiber are also more likely to cause localized tearing as the silicone elongates during impact.

## 3.5 – Conclusion

The methods used for preparing FBG sensing layers were laid out. Three different materials; Kevlar® KM2® Plus, Sorta-Clear 40 silicone, and Smooth-Sil 950 silicone were selected for use in creating sensing layers. The materials were selected based on their flexibility and high strain to failure values. Kevlar® sensing layers were made from a single sheet of plain woven fabric, onto which the FBG was attached using single stitches, placed 3 cm apart. The silicone-based sensing layers were molded into the appropriate shape with the FBG fiber being cast into the center of each sample. In Chapter 4, the impact that sensing layer material and thickness has on

the deformation depth and profile is examined, as well as the ability of each material to ensure FBG survival during impact.

# CHAPTER 4 – Testing and Results

Tests involving Kevlar® and silicone-based sensing layers were performed to study the effectiveness of each material with regards to FBG survivability. The effect of each sensing layer material on the BFD and deformation profile was studied. In addition, for each test involving an FBG, waveform from the FBG was collected and used to determine if/when the FBG fractured.

## 4.1 – Kevlar® Based Sensing Layers

The loosely stitched Kevlar® sensing layers detailed in Chapter 3 were tested using the gas gun setup at NCSU. Prior to testing with the sensing layers and FBG's, baseline tests were performed using shoot packs without any sensing layer placed against the backing material. Five baseline tests were performed in all, each using a 9 mm projectile fired at an average velocity of 360 m/s into a 50-layer Kevlar® shoot pack with heated Roma Plastilina #1 as the backing material.

Tests were then performed in which a "blank" Kevlar® sensing layer was placed behind each shoot pack. The "blank" sensing layers were then tested using the same setup as with the baseline tests. Projectile velocity, deformation width, depth, and volume were recorded using the methods discussed in Chapter 2. The results from the Kevlar® tests were then compared to the baseline tests in order to determine the effect that the Kevlar® sensing layer had on the deformation depth and profile. Table 3 gives the individual results for each of the baseline and Kevlar® tests.

**Table 3:** Baseline and Kevlar® Results.

| Sample # | Velocity (m/s) | Width (mm) | Depth (mm) | Volume (cm^3) |
|---|---|---|---|---|
| **Baseline** | | | | |
| **1** | 351.8 | 47.5 | 32.9 | No Scan |
| **2** | 347.9 | 48.7 | 33.5 | 49.0 |
| **3** | 366.0 | 47.0 | 34.8 | 47.8 |
| **4** | 360.8 | 47.8 | 36.8 | 48.3 |
| **5** | 372.4 | 47.7 | 35.6 | 48.9 |
| **Average** | 359.8 | 47.8 | 34.7 | 48.5 |
| **St. Deviation** | 9.0 | 0.5 | 1.4 | 0.5 |
| **Kevlar** | | | | |
| **1** | 379.1 | 57.3 | 33.4 | 47.4 |
| **2** | 364.9 | 56.2 | 32.1 | 41.4 |
| **3** | 372.4 | 54.8 | 35.9 | 43.2 |
| **4** | 384.8 | 55.3 | 34.6 | 42.8 |
| **5** | 380.2 | 59.1 | 36.1 | 47.8 |
| **Average** | 376.3 | 56.5 | 34.4 | 44.5 |
| **St. Deviation** | 6.9 | 1.5 | 1.5 | 2.6 |

From Table 3, it can be seen that the deformation depth is remained virtually unchanged with the addition of a Kevlar® sensing layer with an average value of 34.7 mm for the baseline and 34.4 for the Kevlar® tests. The average deformation volume of the Kevlar® tests is also slightly lower than that of the baseline. Additionally, the average width increased by 8.7 mm, indicating that the addition of an extra Kevlar® sensing layer had some effect on the final BFD of the clay. It should be noted that the Kevlar® tests had a higher average velocity (376.3 m/s versus 359.8) than the baseline. This is due to inconsistencies in the sabot diameters during testing resulting in the sabot not sealing the barrel perfectly. Switching to a higher quality sabot rectified the issue for future testing. Comparing the depth and volume results from the two Kevlar® and baseline tests with the most closely matching velocities (Baseline 3/Kevlar 2 and Baseline 5/Kevlar 3), it can be seen that the Kevlar® tests did experience a reduction in deformation depth and volume for a given velocity, and a noticeable increase in deformation

width. Figure 35 compares the deformation depth and volume from the baseline tests against the results for the Kevlar® tests.

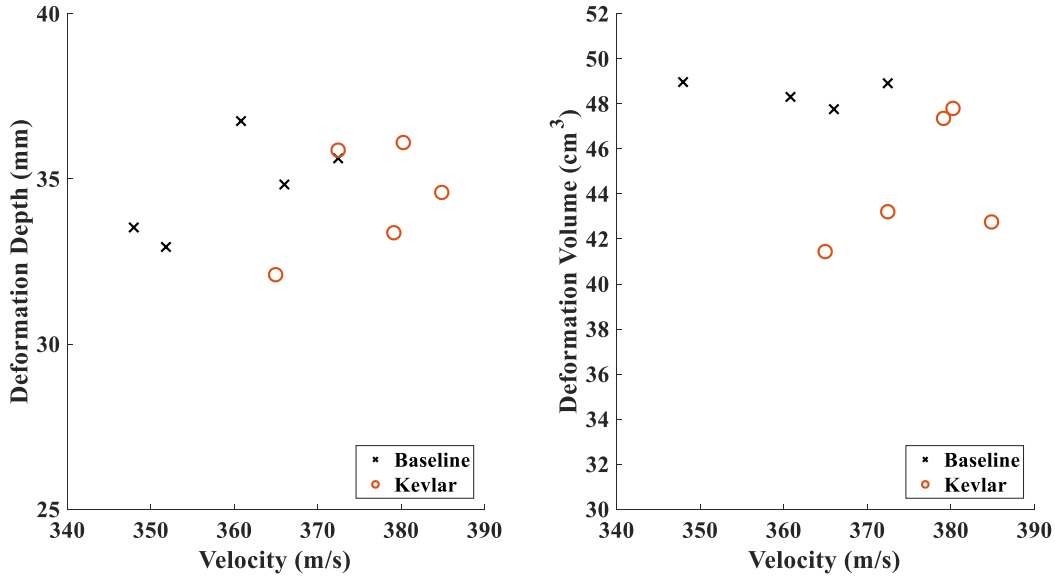


**Figure 35:** Kevlar® Deformation Depth and Volume Comparison.

Figure 35 shows that despite the greater velocity in the Kevlar® tests, the deformation depths are still close to those of the baseline tests. When comparing deformation volumes, the differences are even more clear with the Kevlar® samples showing distinctly lower deformation volumes than the baseline. Figure 36 displays the final deformation profiles of the Kevlar® tests as well as the baseline tests.

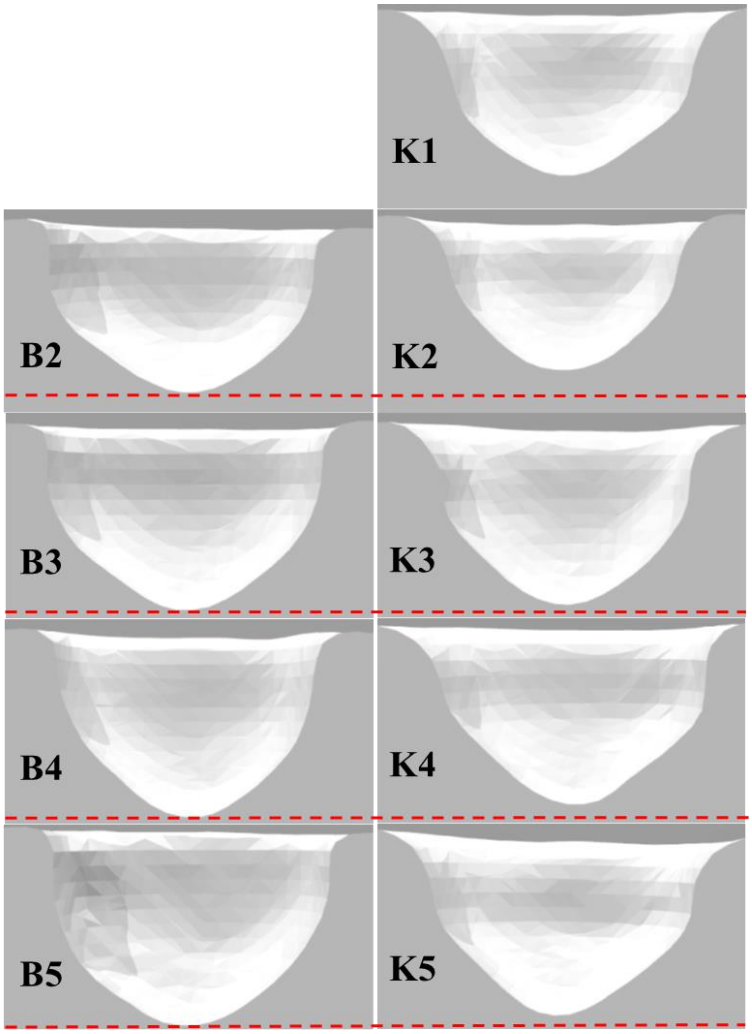


**Figure 36:** Baseline and Kevlar® Deformation Profiles.

From the profiles in Figure 36, it is seen that the tests using a Kevlar® sensing layer exhibit a more tapered profile than that of the baseline tests, in which the deformation shows an abrupt drop close to the edges of the profile. While different in shape, all of the profiles are symmetric for the most part, as would be expected using a symmetric fabric weave.

Further tests were performed in ballistics gelatin to study the change in deformation depth over time when using a Kevlar® based sensing layer. A baseline test was first performed with no sensing layer present. After the baseline data was acquired, a second test was performed using a Kevlar® sensing layer. Side views of the baseline and Kevlar® profiles at several

instances after impact are shown below in Figure 37, where each frame is referenced on how long after impact it occurred.

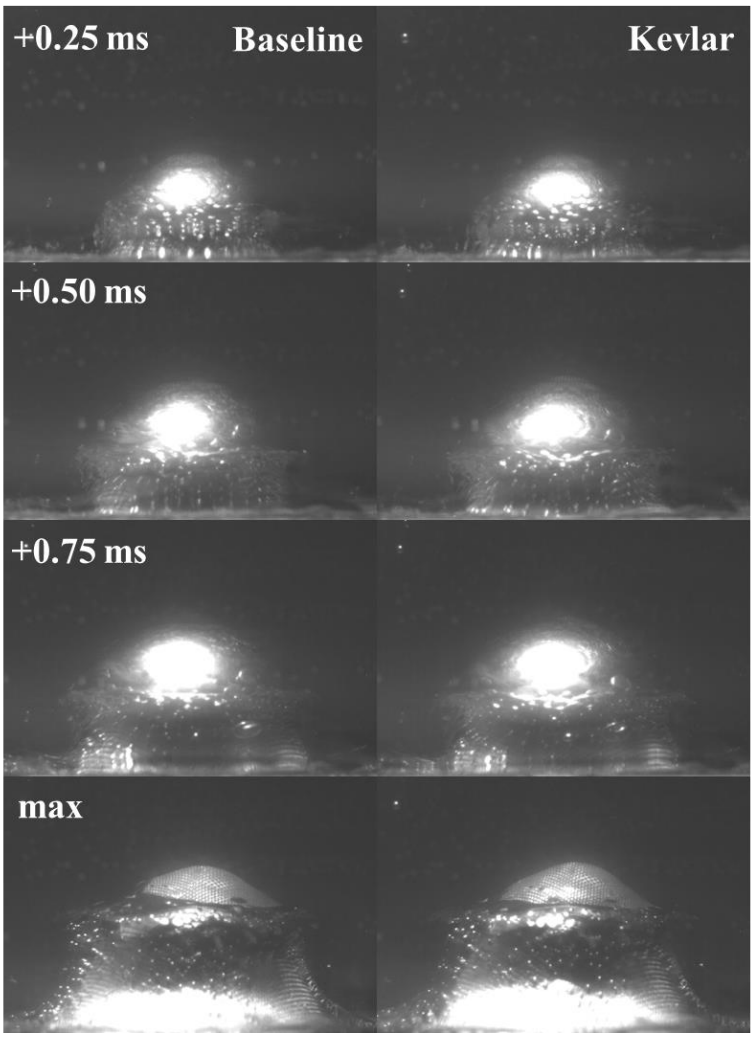


**Figure 37:** Baseline Test (V=403.2 m/s) Versus Kevlar® Test (V=404.5 m/s).

The maximum deformation frame of both the baseline and Kevlar® samples bear a strong resemblance to the profiles seen in the clay testing. During the early stages of the deformation, both profiles appear as smoothly rounded curves. However, as the deformation approaches maximum depth, a ring of entrapped air is seen to form between the backing material and the shoot pack. This ring is likely responsible for the bulge seen midway down the deformation profile in the clay tests. Overall, the baseline and Kevlar® profiles appear very similar. Figure 38

presents the deformation depth over time data gathered during the baseline and Kevlar® tests.

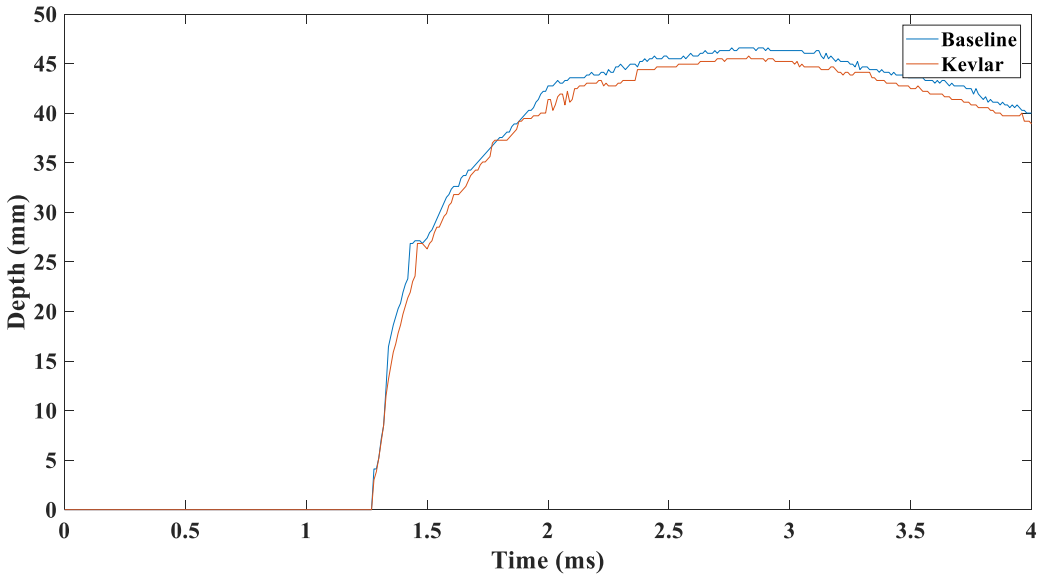


**Figure 38:** Depth Versus Time for Baseline and Kevlar® Samples.

The Kevlar® sample reached a maximum depth of 45.8 mm, compared with a maximum depth of 46.6 mm in the baseline sample. It can be seen that the baseline and Kevlar® curves closely match one another from the beginning of impact up through the point of maximum deformation, which occurs at 2.83 ms for the Kevlar® sample and 2.76 ms for the baseline sample. Although the Kevlar® sensing layer does see a slightly smaller maximum deformation than the baseline, it does not affect the rate at which deformation occurs.

Once the effect of the Kevlar® based sensing layer on the deformation profile and rate of change was known, testing involving Kevlar® sensing layers with embedded FBG's was conducted in order to further study the suitability of Kevlar as a sensing layer. Tests were initially performed using Roma Plastilina #1 modeling clay as the backing material due to the fact that the current standard from personal body armor specifies it as the desired backing material [19]. The samples tested were of the stitched variety discussed in Section 3.2 above. In

accordance with the standard, the clay was heated to roughly 90-100 °F prior to each test. In all, 6 tests were performed on single FBG fibers. Table 4 below gives the individual details for each test.

**Table 4:** Kevlar® FBG Shot Data.

| Sample # | Velocity (m/s) | Depth (mm) |
|---|---|---|
| **Kevlar** | | |
| **1** | 392.0 | 32.8 |
| **2** | 390.8 | 29.6 |
| **3** | 372.4 | 33.4 |
| **4** | 374.6 | 31.2 |
| **5** | 378.0 | 36.6 |
| **6** | 362.9 | 30.5 |
| **Average** | 378.4 | 32.3 |
| **St. Deviation** | 10.2 | 2.3 |

Plots of the FBG strain for each test are given below in Figure 39, each strain value has been converted into a percentage of the maximum recorded strain in order to preserve sensitive data. Note that each time domain has been offset so that impact is occurring at 0 ms on the graph.

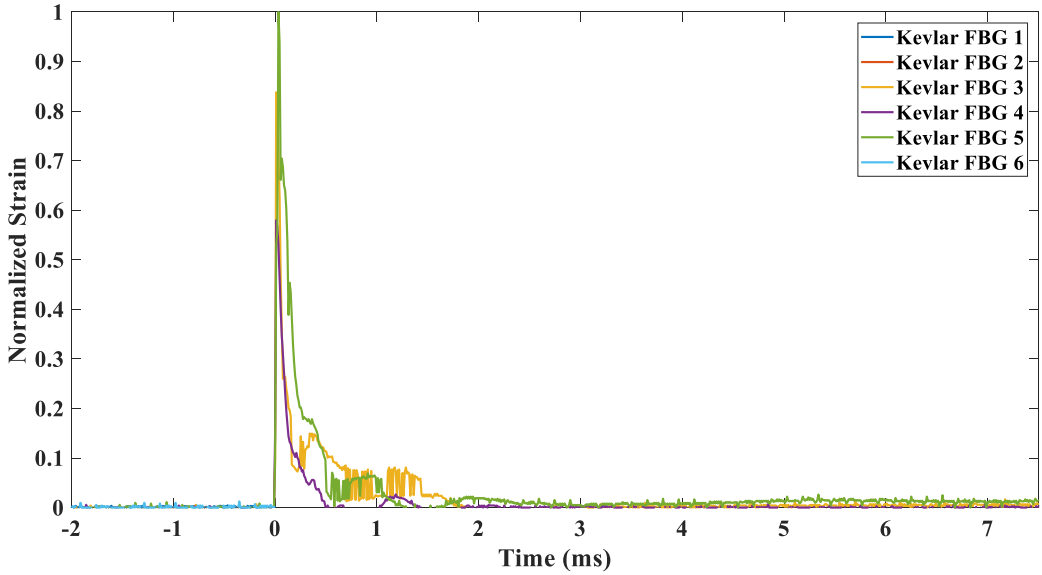


**Figure 39:** Kevlar® FBG Strain.

From the graph, it can be seen that at impact, the FBG sees a large shift in wavelength (and a corresponding jump in strain). Each of the curves in Figure 39 follow a similar strain path during the impact event. An immediate strain spike is seen upon impact, the change in strain is greatest at this point. After the initial spike has occurred, strain relaxation begins to occur as the fiber starts to draw inward with the deformation profile, at which point the strain then quickly falls back to zero. In samples 3 and 5, some noise can be observed in the data as the FBG strain approaches zero. The cause of this noise is unclear but may be due to transmission loss through the fiber resulting in an intensity drop in the waveform voltage.

The fibers in samples 1, 2, and 6 all failed upon impact, as evidenced by the lack of strain data for any time following impact. As previously stated, it is crucial that the FBG sensor be able to survive the projectile impact up until maximum deformation has been reached as this is the period of most interest for the current research involving BABT. Of the 6 tests presented, 3 of the FBG's, or 50%, did not survive the initial impact event. Figure 40 shows a Kevlar stitched sample following testing.

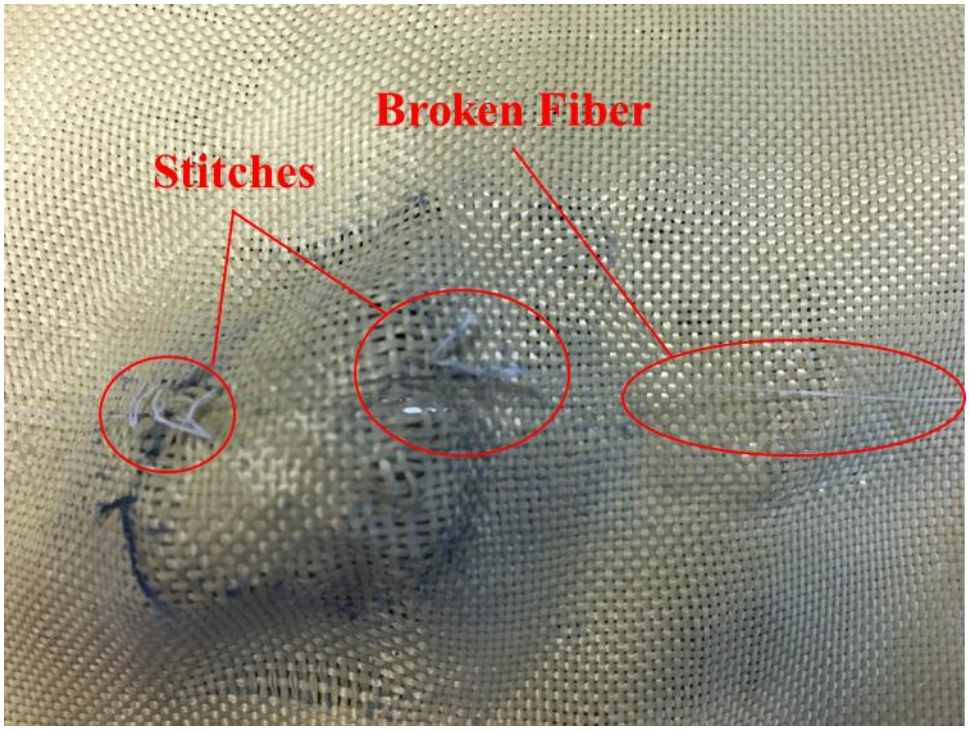


**Figure 40:** Kevlar Stitched Sample After Impact.

It can be seen that the fabric weave becomes very loose during impact as the fibers in the deformation region are stretched. In the test shown in Figure 40, the fiber broke against one of the sow points, which is a common failure mode seen in the Kevlar® samples due to high levels of shear and bending stress seen at the stitches located closest to the deformation.

From the testing discussed above, it appeared that Kevlar® had some promise as a sensing layer material. As seen in Table 4, by reducing the projectile velocity, more of the FBG's survived impact, which was to be expected. Additionally, it was found that by changing the location and tightness of the stitches, fiber survivability could be improved further. Tests 3 and 4 from Table 4 were conducted using loosely stitched samples where the stitch points were placed outside of the expected deformation region. Both of the loosely stitched samples survived throughout impact.

Despite the improvements made to the stitched samples, Kevlar® based sensing layers proved unsuitable for testing in harsher environments after tests were performed at Aberdeen Testing Commons (ATC) in which projectile velocity was increased to a nominal value of 425 m/s and the shoot pack thickness was reduced. All of the Kevlar® mounted FBG's at ATC which were hit directly witnessed fiber failure upon impact. The results from ATC motivated the search for alternative sensing layers materials which could improve fiber survivability.

## 4.2 – 2 mm Silicone Sensing Layers

The 2 mm Sorta-Clear 40 and Smooth-Sil 950 silicone sensing layers described in Chapter 3 were tested using the high-speed gas gun set up at NCSU. Silicone samples without an embedded FBG were fabricated for initial testing. As with the Kevlar sensing layers, the blanks were tested using 9 mm projectiles fired into a 50-layer shoot pack with warmed clay as the backing material. 5 samples of each type of silicone were tested originally, for a total of 10 samples. Table 5 presents the detailed shot information for the 2 mm silicone samples as well as details from the baseline tests in Section 4.1, for comparison.

**Table 5:** 2 mm Sorta-Clear 40 and Smooth-Sil 950 Shot Details.

| Sample # | Velocity (m/s) | Width (mm) | Depth (mm) | Volume (cm^3) |
|---|---|---|---|---|
| **Baseline** | | | | |
| **1** | 351.8 | 47.5 | 32.9 | No Scan |
| **2** | 347.9 | 48.7 | 33.5 | 49.0 |
| **3** | 366.0 | 47.0 | 34.8 | 47.8 |
| **4** | 360.8 | 47.8 | 36.8 | 48.3 |
| **5** | 372.4 | 47.7 | 35.6 | 48.9 |
| **Average** | 359.8 | 47.8 | 34.7 | 48.5 |
| **St. Deviation** | 9.0 | 0.5 | 1.4 | 0.5 |
| **Smooth-Sil 2mm** | | | | |
| **1** | 359.8 | 53.5 | 33.6 | 44.2 |
| **2** | 364.9 | 56.5 | 33.9 | No Scan |
| **3** | 379.1 | 56.7 | 31.7 | 41.0 |
| **4** | 361.8 | 54.9 | 34.8 | 43.1 |
| **5** | 368.1 | 54.2 | 33.1 | 37.4 |
| **Average** | 366.8 | 55.2 | 33.4 | 41.4 |
| **St. Deviation** | 6.8 | 1.3 | 1.0 | 2.6 |
| **Sorta-Clear 2 mm** | | | | |
| **1** | Bad Trigger | 51.9 | 35.8 | 44.3 |
| **2** | 361.8 | 51.4 | 29.2 | 36.7 |
| **3** | 367.1 | 52.1 | 33.3 | 41.7 |
| **3** | 363.9 | 54.6 | 29.2 | 39.2 |
| **4** | 366.0 | 52.2 | 36.1 | 45.5 |
| **Average** | 364.7 | 52.4 | 32.7 | 41.5 |
| **St. Deviation** | 2.0 | 1.1 | 3.0 | 3.2 |

Comparing the silicone results against that baseline shows that both the Sorta-Clear 40 and Smooth-Sil 950 samples had an appreciable impact on the final deformation dimensions in the clay. For the Smooth-Sil samples, the deformation width increased by an average of 7.4 mm while the depth decreased by an average of 1.3 mm. As with the Kevlar® samples, despite the average recorded width increasing more than the depth, the deformation volume dropped by 7.1 $cm^3$ on average. The results of the Sorta-Clear 2 mm tests show a similar trend to that of the Smooth-Sil. Average width increased by 4.6 mm over the baseline results while the average

depth decreased by 2.0 mm. As with the Smooth-Sil tests, despite the greater increase in width, the average volume decreased by 7.0 $cm^3$. These results indicate that the final deformation volume is more strongly influenced by the depth of deformation, rather that the deformation width. To supplement the information in Table 5, a comparison of the deformation depth and volume against the projectile velocities is given below in Figure 41.

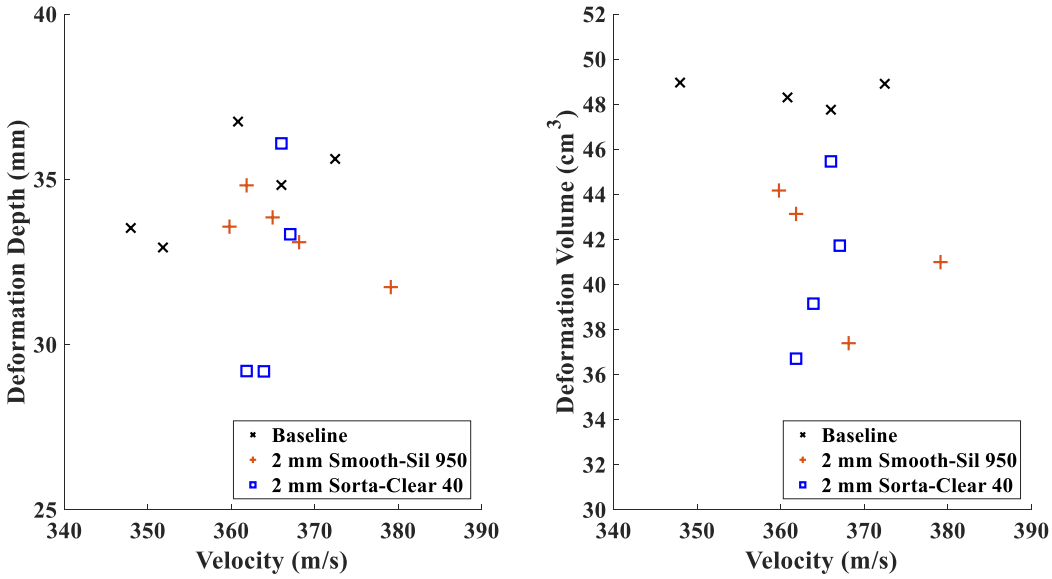


**Figure 41:** 2 mm Silicone Deformation Depth and Volume Comparison.

Figure 41 shows that the addition of a 2mm thick silicone layer results in reduced deformation depth and volume versus the baseline tests. Overall, it can be seen that although the change in depth in both silicone types was relatively small, it did have an effect on the volume of the BFD. This change in volume may lead to an impact when attempting to verify BABT models. Figure 42 gives cross-sections of each of the scanned deformations from the 2 mm silicone and baseline tests.

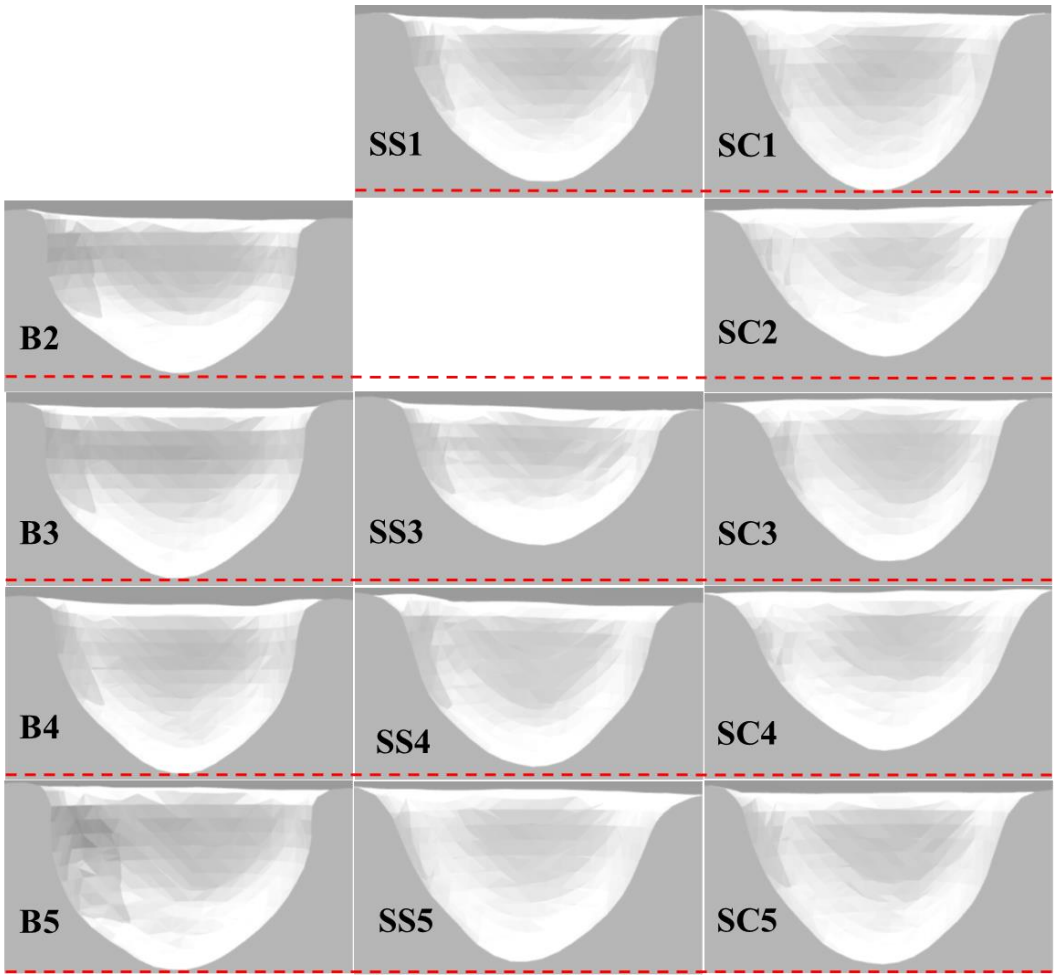


**Figure 42:** Deformation Profiles for Baseline (B), 2 mm Smooth-Sil (SS), and 2 mm Sorta-clear (SC).

Figure 42 shows that while the deformation is wider at the surface of the modeling clay for each of the 2 mm silicone tests, the general profile of the deformation remains very similar to the baseline, with only a slightly more rounded profile being seen. This behavior can be observed for all of the 2 mm silicone tests, regardless of the silicone type.

To better study how the 2 mm silicone affected the deformation depth during impact, Sorta-Clear and Smooth-Sil samples were tested against a ballistics gelatin backing material to allow for high speed imaging of the profile. The results where then compared against the baseline ballistics gelatin test given in Section 4.1. Figure 43 below gives side profile views of the deformation at various times after impact.

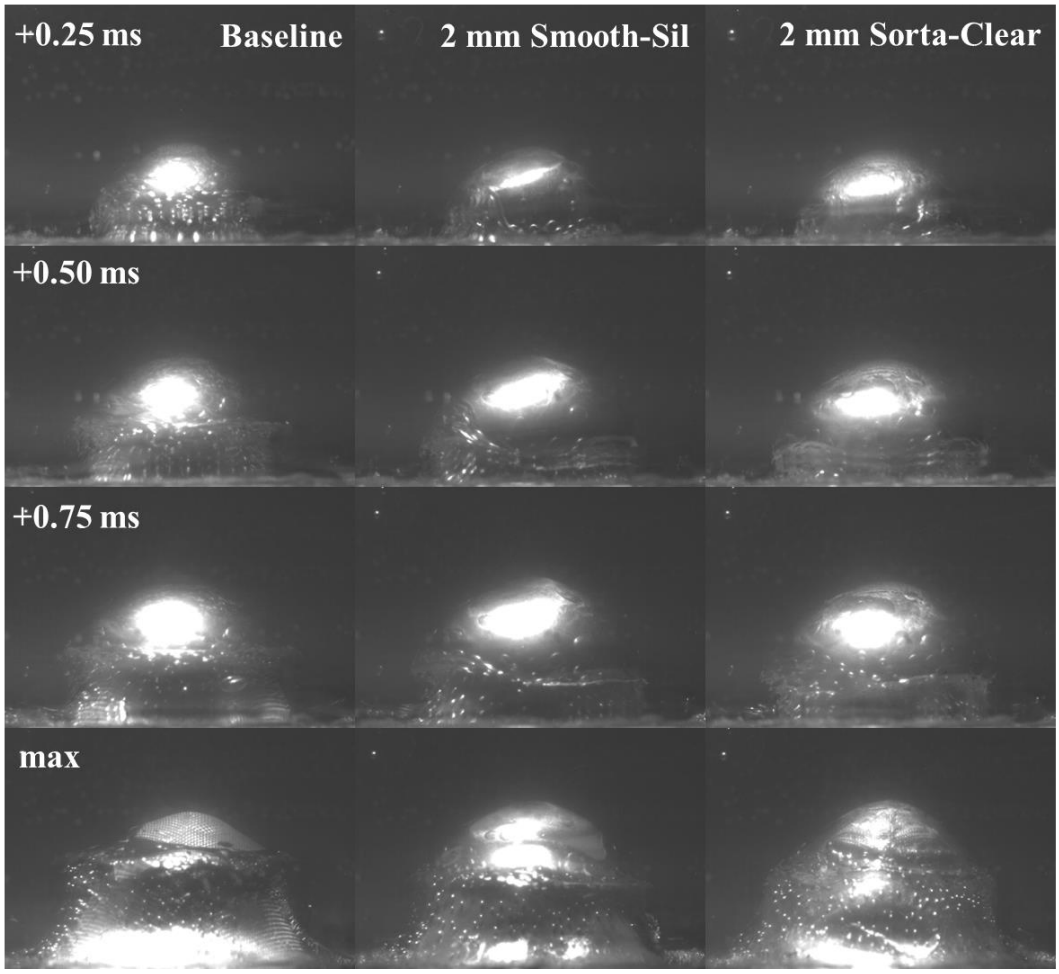


**Figure 43:** Baseline (403.2 m/s), 2 mm Smooth-Sil (V=400.6 m/s), and 2 mm Sorta-Clear (V=403.2 m/s).

The 2 mm samples exhibited similar profiles during impact. In the initial frames of the impact, the deformation shape remains roughly semicircular as the shoot pack layers wrap around the projectile. As the impact progresses, it can be seen that the two silicone samples had a more rounded end than the baseline. Interestingly, neither of the silicone samples developed the ring of trapped air seen in both the baseline and Kevlar® samples. The time dependent depth results for the 2 mm test above are given in Figure 44.

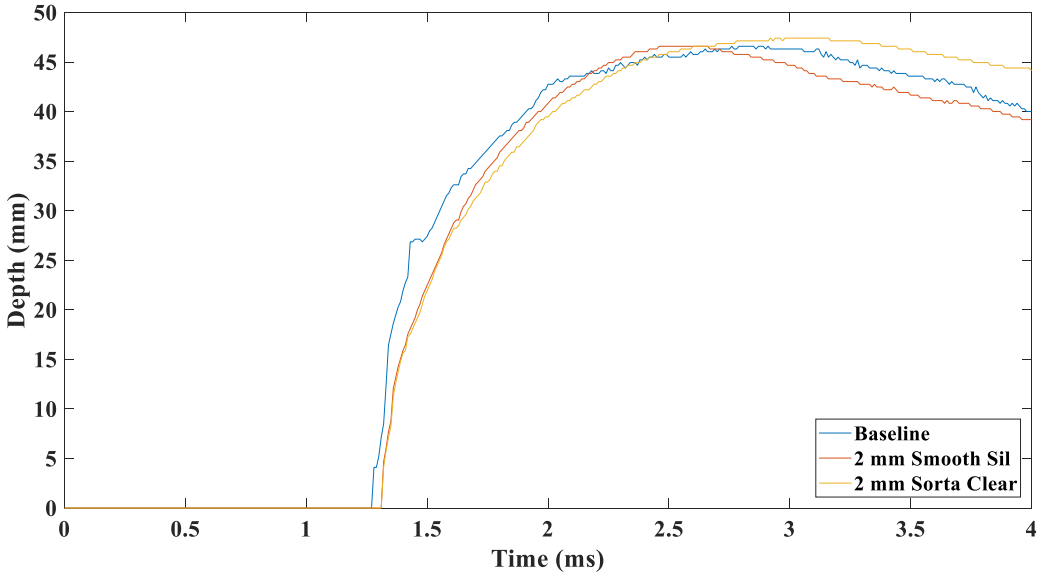


**Figure 44:** Depth Versus Time for Baseline and 2 mm Silicone Samples.

Both of the 2 mm samples showed a similar depth versus time curve to that of the baseline gelatin shot. The Sorta-Clear did exhibit a slightly slower rise time to maximum depth than the Smooth-Sil sample however, with maximum depth occurring at 2.60 ms for the Smooth Sil sample and 2.92 ms for the Sorta-Clear.

The 2 mm silicone samples were then tested with embedded fibers to observe their effects on the survivability of the FBG. 3 Sorta-Clear 40 and 1 Smooth-Sil 950 samples were created and tested. One of the Sorta-Clear samples was also coated in a layer of Vaseline® prior to being cast in the silicone. The purpose of this was to study the effect that a coating of lubricant had on the maximum strain observed on an FBG embedded within a silicone layer. The tests were then performed using the same set up as the Kevlar FBG testing in Section 4.1. The shot details for the 2 mm FBG tests are given below in Table 6.

**Table 6:** Shot Details for 2 mm Silicone FBG Tests.

| Sample # | Velocity (m/s) | Depth (mm) |
|---|---|---|
| **2 mm Smooth-Sil** | | |
| **1** | 404.5 | 39.6 |
| **2 mm Sorta-Clear** | | |
| **1** | 408.4 | 38.9 |
| **2** | 396.9 | 37.5 |
| **3** | 399.4 | 30.6 |
| **Average** | 401.5 | 35.7 |
| **St. Deviation** | 4.9 | 3.6 |

The Sorta-Clear 3 sample from Table 6 is the FBG which was coated in Vaseline® prior to being placed in the silicone mold while the other samples were all cured without any lubricant coating. Figure 45 gives the normalized strain data collected from each FBG during impact.

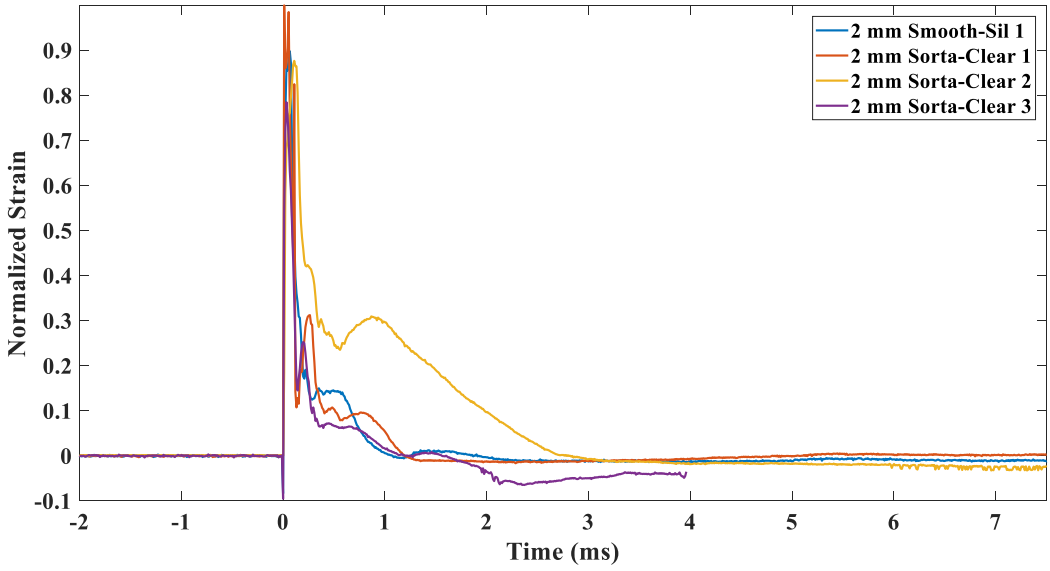


**Figure 45:** 2 mm Silicone FBG Strain.

The results from the silicone samples were promising, as all 4 fibers survived through impact and were able to collect data. Note that the Sorta-Clear 3 sample did break as it was pulled against the corner of the testing block, but the break was not in the impact zone and

happened well after maximum deformation had been reached. For each test it can be seen that the strain spikes as soon as impact occurs and quickly reaches a maximum value, similar to the Kevlar® samples. Following the initial strain spike, the strain in the FBG takes much longer to fully relax than the Kevlar® samples. This is due to the fact that the silicone grips the entire embedded length of the fiber, resulting in a larger friction force on the fiber as it slips, compared to the Kevlar® stitched samples which have very few contact points with the fiber. The increased interaction between the FBG and the silicone also resulted in the grating experiencing a higher overall strain when compared with the Kevlar® samples. The Vaseline® coated Sorta-Clear 3 sample showed a slight reduction in the maximum strain value as well as a quicker strain relaxation period than the other, non-lubricated samples, indicating that the kinetic friction coefficient between the fiber and silicone had been reduced. Figure 46 shows a 2 mm Sorta-Clear sample with an embedded fiber after it had been impacted.

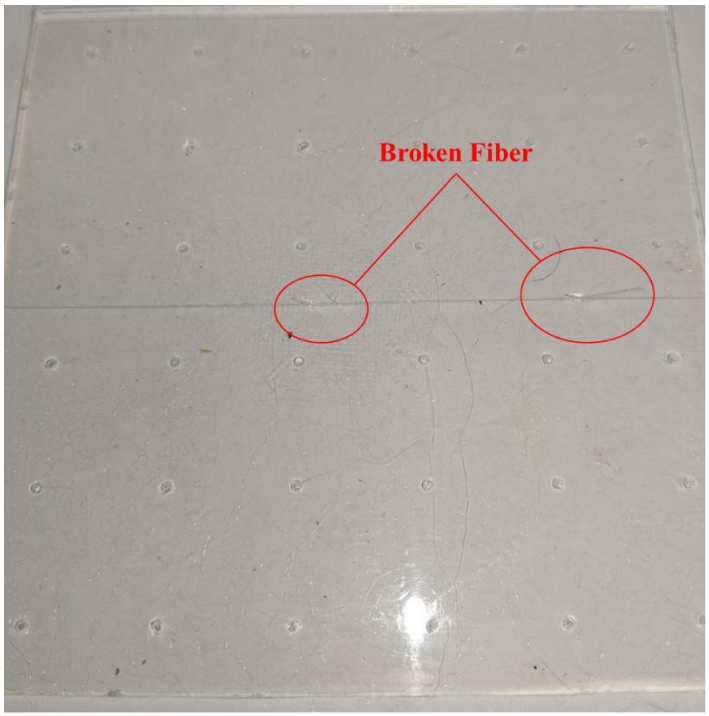


**Figure 46:** 2 mm Sorta-Clear Sample After Impact.

Figure 46 illustrates a common type of fiber failure seen in the 2 mm silicone samples. It can be seen that although the silicone sensing layer itself remains undamaged, there are shards of broken optical fiber which have poked through the silicone. The fiber breakage is due to buckling in the fiber as the silicone layer rebounds from maximum deformation. Figure 47 shows a still frame of a fiber buckling during rebound.

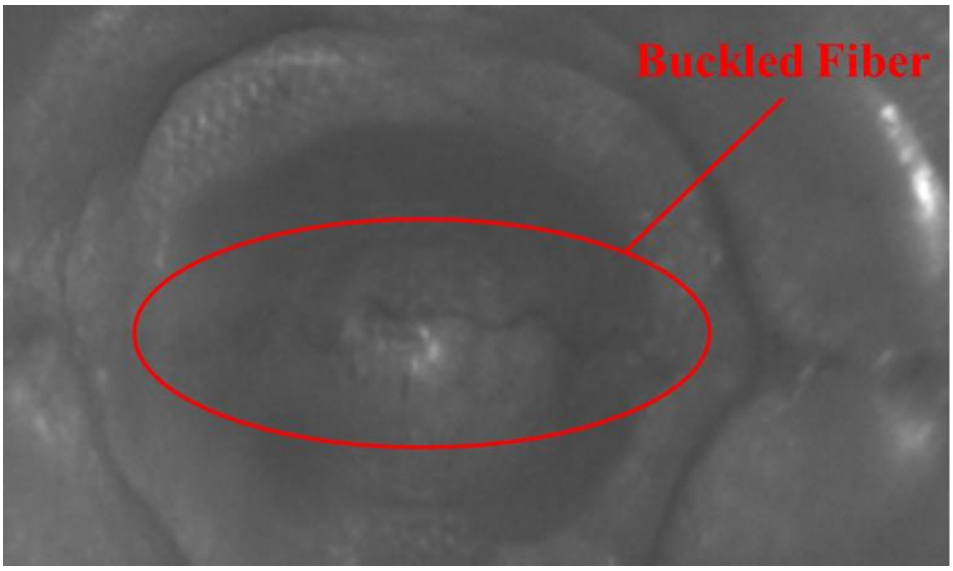


**Figure 47:** Fiber Buckling During Rebound.

The fiber buckling is due to the fact that as the silicone layer gets strained by the projectile, it draws more of the fiber length into the sensing layer. Once the silicone has reached maximum deformation, it then starts to contract elastically back to its original shape. However, the extra fiber length becomes bound up within the silicone and cannot escape, resulting in the buckling pattern seen in Figure 47. Although this does often result in the fiber breaking, since the breakage occurs well after both impact and maximum deformation, the FBG is still able to record significant data.

From the testing results for the Sorta-Clear 40 and Smooth-Sil 950 materials, silicone-based sensing layers appear to be a suitable replacement for the Kevlar® based sensing layers.

All 4 of the FBG samples tested in 2 mm silicone survived through impact, demonstrating that the silicone can adequately protect the fiber from abrasion and strain to failure during testing. There were no appreciable differences observed between the two types of silicone, Sorta-Clear 40 and Smooth-Sil 950. Both types performed similarly to one another. However, due to the fact that Sorta-Clear 40 produces a transparent sensing layer, it is more suitable for testing involving ballistics gelatin as the embedded fiber can be visually tracked during testing.

While the silicone performed well in terms of FBG survivability, the deformation tests conducted show that the 2 mm thick samples have more of an impact on the BFD than the Kevlar based sensing layers. Since shoot pack thickness is approximately 8.5 mm for a 50-layer pack, the 2 mm silicone added significantly to the overall thickness of the material in front of the backing material, which resulted in wider more shallow deformations.

## 4.3 – 1 mm Silicone Sensing Layers

In order to reduce the impact that the silicone sensing layers had on the deformation dimensions, the silicone sensing layer thickness was reduced to approximately 1 mm. Testing was conducted in the same manner as with the Kevlar and 2 mm silicone samples. 2 samples of Sorta-Clear 40 and 2 samples of Smooth-Sil 950 were tested in modeling clay to study the effect on final deformation dimensions. Table 7 gives the shot details for each of the samples.

**Table 7:** 1 mm Sorta-Clear 40 and Smooth-Sil 950 Shot Details.

| Sample # | Velocity (m/s) | Width (mm) | Depth (mm) | Volume (cm^3) |
|---|---|---|---|---|
| **Baseline** | | | | |
| **1** | 351.8 | 47.5 | 32.9 | No Scan |
| **2** | 347.9 | 48.7 | 33.5 | 49.0 |
| **3** | 366.0 | 47.0 | 34.8 | 47.8 |
| **4** | 360.8 | 47.8 | 36.8 | 48.3 |
| **5** | 372.4 | 47.7 | 35.6 | 48.9 |
| **Average** | 359.8 | 47.8 | 34.7 | 48.5 |
| **St. Deviation** | 9.0 | 0.5 | 1.4 | 0.5 |
| **1 mm Smooth-Sil** | | | | |
| **1** | 368.1 | 54.8 | 37.9 | 48.7 |
| **2** | 372.4 | 54.7 | 35.7 | 45.2 |
| **Average** | 370.3 | 54.7 | 36.8 | 46.9 |
| **St. Deviation** | 2.2 | 0.0 | 1.1 | 1.7 |
| **1 mm Sorta-Clear** | | | | |
| **1** | 362.9 | 50.9 | 34.4 | 42.4 |
| **2** | 366.0 | 56.5 | 33.9 | 51.7 |
| **Average** | 364.4 | 53.7 | 34.1 | 47.1 |
| **St. Deviation** | 1.6 | 2.8 | 0.3 | 4.7 |

The data above shows that the 1 mm silicone samples had less of an impact on the final deformation of the clay than the 2 mm samples, as expected. In the case of the 1 mm Smooth-Sil, average width increased by 6.9 mm, versus 7.4 mm for the 2 mm Smooth-Sil. Unexpectedly, the average deformation depth of the Smooth-Sil increased from the baseline value. This can be attributed to a difference in the clay stiffness as it is highly dependent on the temperature of the testing block. The deformation volume of the Smooth-Sil showed only a slight decrease against the baseline, an average of 1.6 $cm^3$. The Sorta-Clear samples displayed deformation width and volume results similar to that of the Smooth-Sil. The average width increased by 5.9 mm from the baseline. Average depth decreased slightly by 0.6 mm. And the deformation volume also decreased 1.4 $cm^3$. Figure 48 compares the deformation depth and volume from the tests shown in Table 6 against the measured projectile velocities.

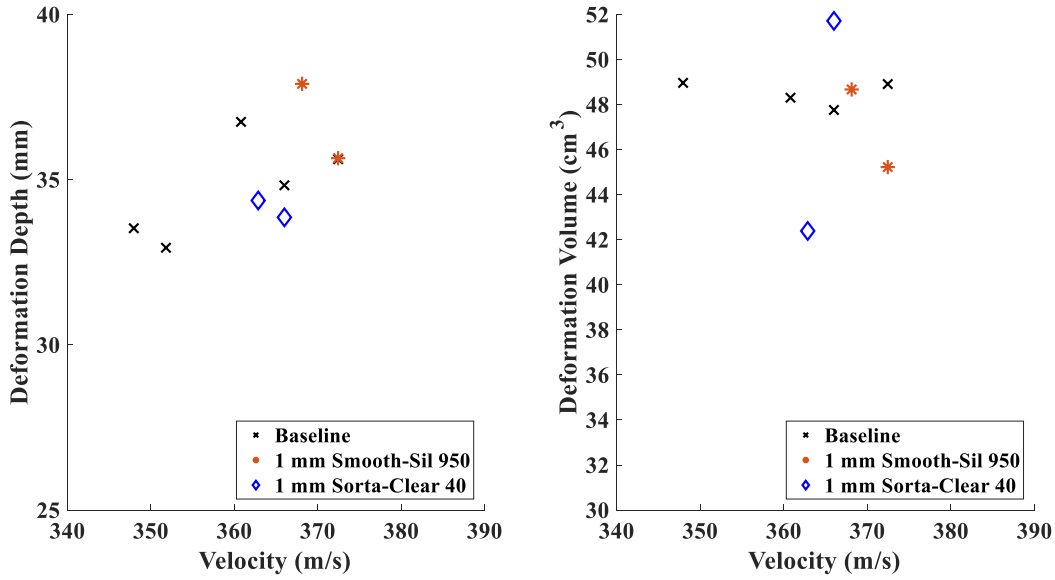


**Figure 48:** Kevlar Deformation Depth and Volume Comparison.

Other than the Smooth-Sil sample which showed an abnormally large deformation depth, the depth values from the 1 mm silicone samples closely matched that of the baseline with only a slight reduction. The Sorta-Clear samples saw a larger variability in the deformation volume than expected, likely due to the differences in clay stiffness already discussed. Figure 49 displays the final deformation cross sections of each of the 1 mm samples, as well as the cross sections of the baseline samples.

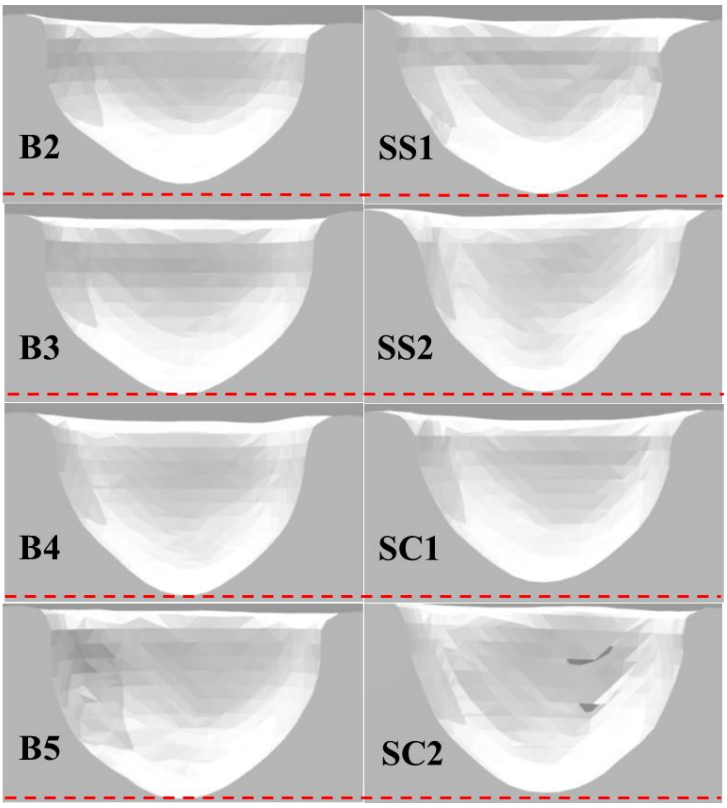


**Figure 49:** Deformation Profiles for Baseline (B), 1 mm Smooth-Sil (SS), and 1 mm Sorta-Clear (SC).

The cross sections of each of the 1 mm specimens closely resembles that of the baseline samples with each profile having the slightly pointed end and bulged midsection seen in the baseline tests.

High speed cameras were used with a ballistics gelatin backing to record the deformation profile exhibited when a 1 mm silicone sensing layer was in place. Figure 50 gives the profile of 1 mm Smooth-Sil and Sorta-Clear samples being impacted behind a 50-layer shoot pack.

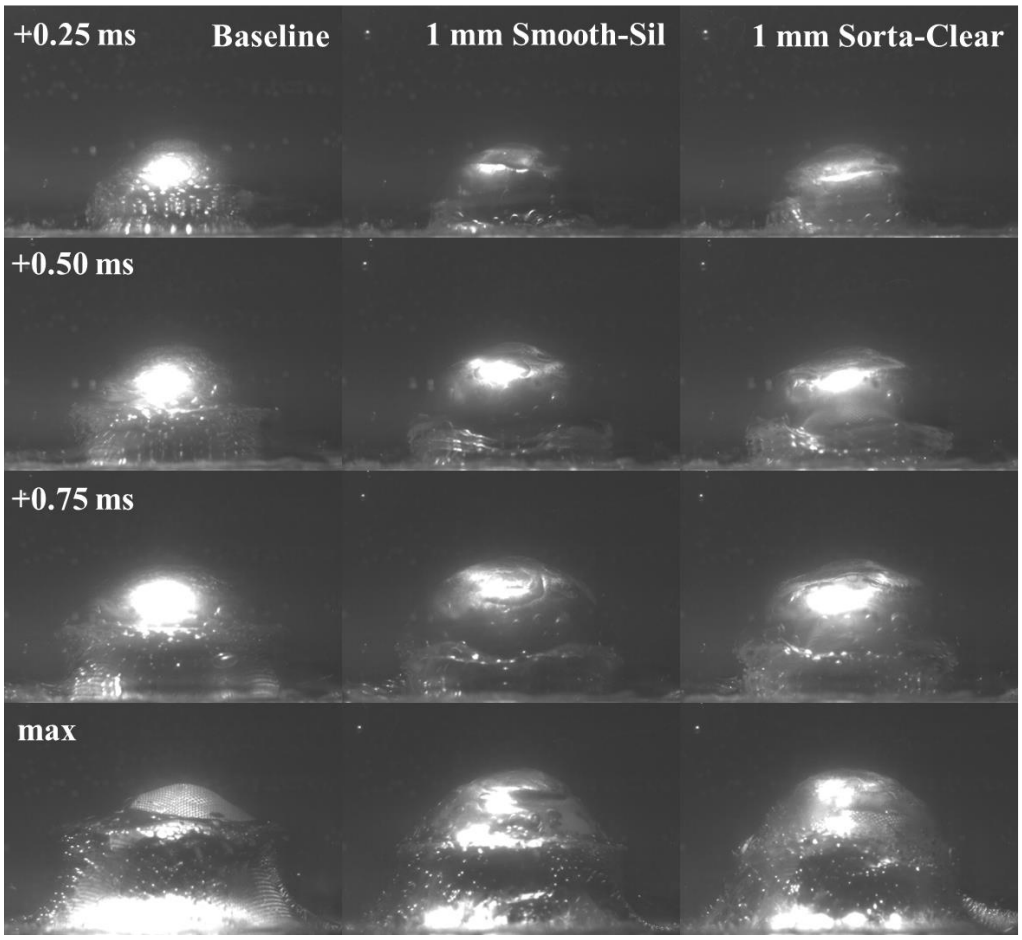


**Figure 50:** Baseline (V=403.2 m/s), 1 mm Smooth-Sil (V=400.6 m/s), and 1 mm Sorta-Clear (V=400.6 m/s).

From the figure, the Smooth-Sil and Sorta-Clear samples both show similar profiles during deformation. As with the 2 mm silicone tests, the 1 mm sensing layers do not appear to form the distinct overhung region caused by trapped air which the baseline displays. The depth over time data for both of the 1 mm samples is given below in Figure 51.

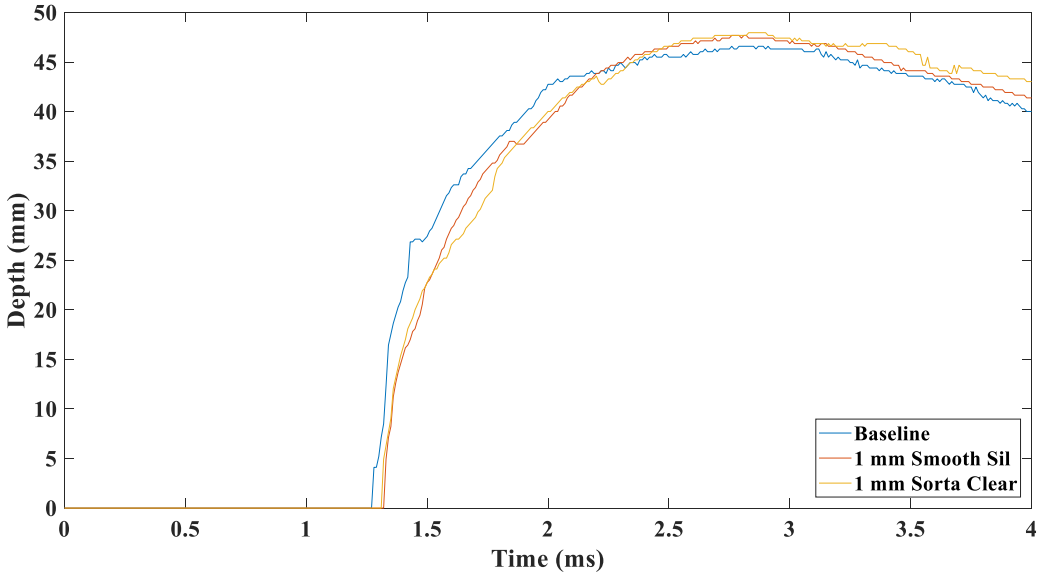


**Figure 51:** Depth Versus Time for 1 mm Silicone Samples and Baseline.

As with the Kevlar and 2 mm samples, the depth versus time curves of the 1 mm silicone aligns closely with that of the baseline. The silicone samples reached maximum depth at 2.76 ms for the Smooth-Sil and 2.83 ms for the Sorta-Clear. The Sorta-Clear sample was again seen to have a slower deformation time than that of the Smooth-Sil.

Finally, to test the survivability of FBG's within 1 mm thick silicone, 5 new samples were created, 1 made from Smooth-Sil 950 and 4 made from Sorta-Clear 40. The first Smooth-Sil sample was tested in clay and the remaining 4 samples were tested against a ballistics gelatin backing. All of the 1 mm samples were coated in Vaseline® prior to being cast in silicone and the fiber was broken loose in the sensing layer by pulling the fiber back and forth within the channel in order to reduce the maximum strain value on the fiber.

It should also be noted that the test setup was adjusted for the 1 mm FBG testing. In an attempt to better mimic the dynamics seen at Aberdeen Testing Commons (ATC), where future body armor testing will occur, the test setup at NCSU was altered, as detailed in Table 8.

**Table 8:** NCSU Test Setup Changes.

| | Projectile Type | Nominal Velocity (m/s) | Shoot Pack Thickness (layers) |
|---|---|---|---|
| **Previous Test Setup** | 9 mm | 400 | 50 |
| **New Test Setup** | 9 mm | 425 | 30 |

While the projectile remained the same, the velocity was increased significantly and the shoot pack thickness was reduced by approximately 3.4 mm. Table 9 details the individual information for each of the 1 mm silicone FBG tests performed.

**Table 9:** Shot Details for 1 mm Silicone FBG Tests.

| Sample # | Velocity (m/s) | Depth (mm) |
|---|---|---|
| **1 mm Smooth-Sil** | | |
| **1** | 423.3 | 52.7 |
| **1 mm Sorta-Clear** | | |
| **1** | 420.5 | 53.0 |
| **2** | 413.7 | 55.7 |
| **3** | 427.6 | 44.6 |
| **4** | 423.3 | 40.8 |
| **Average** | 421.3 | 48.5 |
| **St. Deviation** | 5.1 | 6.0 |

As expected, the new testing parameters resulted in a larger BFD in the backing material when compared to the Kevlar and 2 mm Silicone samples. Figure 52 below shows the strain results from the 1 mm silicone tests in clay and ballistics gelatin.

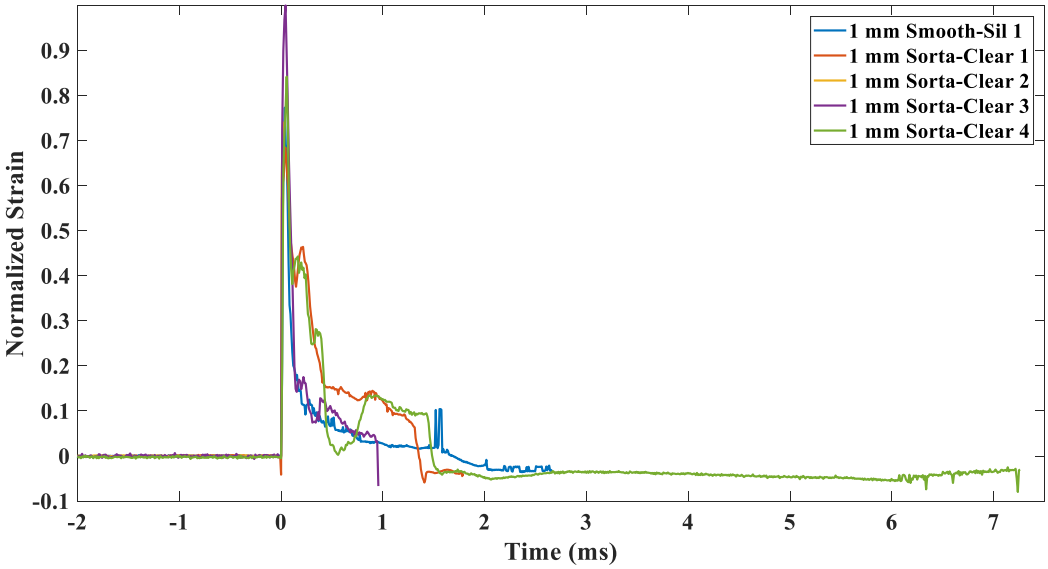


**Figure 52:** 1 mm Silicone Strain.

The 1 mm silicone embedded FBG's showed a similar strain profile to that of the 2 mm FBG's. The strain spikes quickly upon impact, as with the other FBG's tested. However, the silicone samples did show a unique secondary strain spike well after impact had occurred that was not seen in the Kevlar samples, which decayed smoothly after the initial spike. Figure 53 displays the differences between the different silicone and Kevlar® FBG strain profiles.

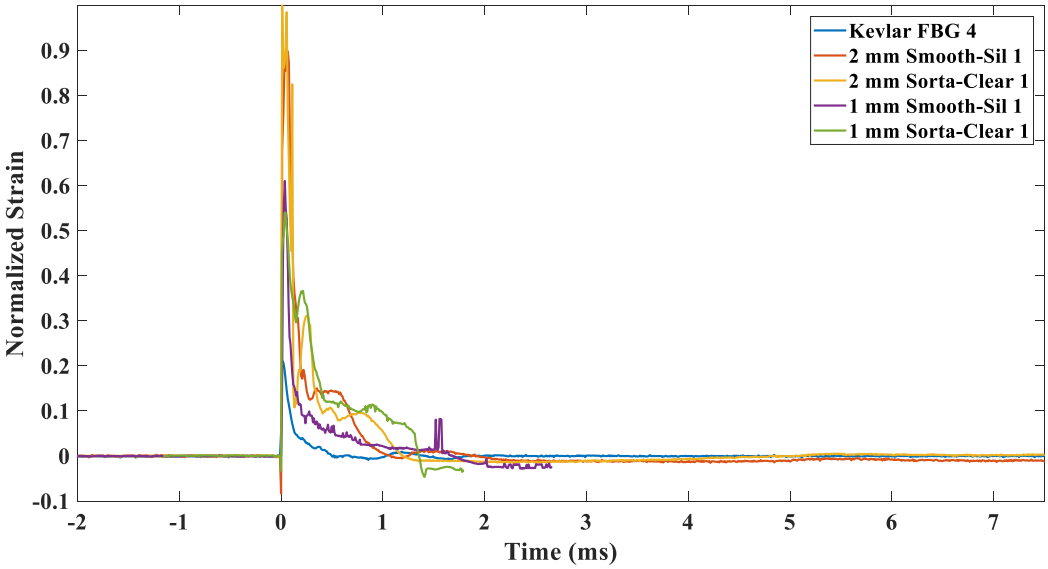


**Figure 53:** Strain Profile Comparison.

From the figure above, the differences between Kevlar® based sensing layers and silicone-based sensing layers becomes more apparent. The secondary jump in strain is seen in each of the silicone samples, regardless of Vaseline® coating or sample thickness. This secondary spike in the strain is likely due to the fiber sticking against the silicone at some point along its length. It can also be seen that the Vaseline® coating resulted in the 1 mm FBG's recording a lower maximum strain than the 2 mm samples, both of which were uncoated. The strain in the silicone samples was still higher than that of the Kevlar®, however, since the stitched fibers could much more easily slip.

The 1 mm silicone tests displayed good results in terms of FBG survivability, despite the increased test dynamics and reduced layer thickness. Of the 5 samples tested, 4 survived past impact, or 80%. In the one test that did not survive impact, Sorta-Clear 2, the fiber broke externally to the sensing layer rather than at the impact area. It is believed that the fiber was

pulled taut against the edge of the testing block as it was drawn in during impact, causing it to break. Figure 54 shows a 1 mm Sorta-Clear sample after being impacted.

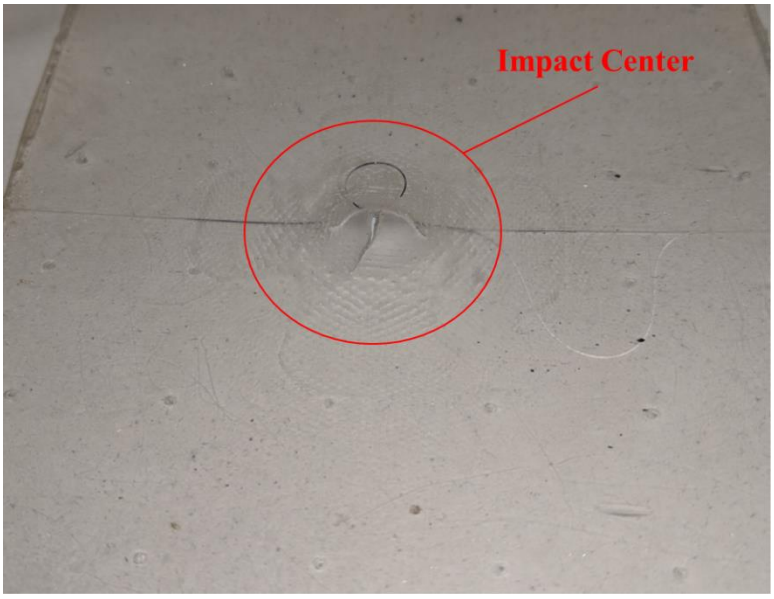


**Figure 54:** 1 mm Sorta-Clear Samples After Impact.

Clearly the 1 mm silicone sustained significantly more damage than the 2 mm sample shown in Section 4.2. It can be seen that the fiber also burst loose from the sensing layer at several points along the length as it was impacted. Surprisingly, the damage to the sensing layer served to reduce fiber breakage along the embedded fiber length. Since the sensing layer splits at the impact center, the fiber is not trapped within the silicone as it rebounds, enabling it to coil against itself rather than kinking and breaking as seen in the 2 mm samples.

## 4.3 – Conclusions

Kevlar, 2 mm silicone, and 1 mm silicone samples were tested to examine each sensing layers effects on the BFD. Additionally, each material was tested using an attached FBG to determine how effectively they could protect the fiber during impact. 2 types of silicone were

used, Smooth-Sil 950 and Sorta-Clear 40. All of the samples were tested using 9 mm FMJ projectiles.

Results from the deformation testing showed that each of the different sensing layers had some impact on the final dimensions of the backing material. For each sensing layer material and thickness, the overall deformation width increased when compared to baseline samples with no sensing layer present. Each material also resulted in a reduction in deformation depth and volume, with the exception of the 1 mm Smooth-Sil samples. The 2 mm silicone samples displayed the largest overall effect on the deformation dimensions.

Of the materials and configurations tested, the 1 mm Sorta-Clear samples proved to be the best candidate for future testing. The reduced thickness resulted in a smaller impact on the BFD when compared to the 2 mm thick samples, which caused noticeable reductions in both the deformation depth and volume. In terms of fiber survivability, the 1 mm sensing layers outperformed the Kevlar® based ones, even with increased test dynamics. Finally, since the Sorta-Clear samples were transparent, it was possible to directly image the fiber during impact using high speed cameras.

# CHAPTER 5 – Conclusions and Future Work

In this chapter, conclusions drawn from the testing results of Kevlar and Silicone based sensing layers are discussed and ideas for future objectives are given.

## 5.1 – Conclusions

Three different materials; Kevlar® KM2® Plus, Smooth-Sil 950 platinum cure silicone, and Sorta-Clear 40 platinum cure silicone were studied to determine the most appropriate material for use as an FBG sensing layer. Silicone layers made from 1 mm thick Sorta-Clear 40 silicone were found to be effective at both protecting embedded FBG sensors during high speed ballistic impact and avoiding any significant effect on the BFD.

Using the experimental setup described in Chapter 2, it was possible to measure final deformation depth, width, and volume in a Roma Plastilina #1 backing material. High speed cameras used in conjunction with clear 20% NATO standard ballistics gelatin also made it possible to measure the deformation depth and width during impact [21]. Finally, information collected from optical fibers containing FBG's was used to determine whether or not the optical fibers survived impact. The complete results gave insight into how each material affected the BFD of the backing material as well as how effective the material was at ensuring that the FBG sensor successfully collected data throughout impact. The information obtained enables the production of robust sensing systems for future body armor testing to help study the effect of BABT on individuals. In particular it was found that:

1. The addition of any type of sensing layer increased the deformation width while decreasing deformation depth and volume, when shoot pack thickness and projectile velocity was held constant.

2. The thickness of the sensing layer has a large effect on the final deformation dimensions as reducing the silicone sensing layer thickness from 2 to 1 mm resulted in a 1-2 mm increase in the deformation depth and a 5-6 $cm^3$ increase in deformation volume.
3. Stitching the optical fiber onto a Kevlar® sensing layer allowed the fiber to slip easily as the sensing layer was drawn in but the stitch points acted as localized stress risers and resulted in a large number of fiber breakages immediately following impact.
4. Encasing the fiber in silicone eliminated the issue of stress concentrations at the stitch points and greatly increased fiber survivability.
5. Coating the fiber in a Vaseline® lubricant prior to embedding it in the silicone, served to reduce the friction coefficient between the fiber and silicone and in turn reduced the maximum strain seen on the fiber.

In summary, the 1 mm Sorta-Clear silicone proved to be the ideal candidate for future testing. Both of the silicone materials tested were superior to the Kevlar® in terms of fiber survivability. Reducing the silicone thickness from 2 mm to 1 mm resulted in a lesser impact on the BFD while still maintaining good fiber survivability. Finally, the Sorta-Clear silicone was favorable to the Smooth-Sil as it allowed for the fiber to be directly imaged during impact.

## 5.2 – Future Work

Despite the steps made towards producing a reliable measurement system to study the effects of BABT, there are still several areas which need improvement.

1. Testing a larger number of samples for each sensing layer would be beneficial as it would provide more accurate data regarding each different material's effect on the deformation.

2. Testing samples in which multiple optical fibers are embedded is important for any future efforts to create a model for determining injury due to BABT as it would allow for reconstruction of the deformation shape.
3. Currently, all of the samples tested have only been suitable for a single test. During impact, the optical fiber often loses its protective coating due to abrasion and further impacts result in fiber failure. Efforts should be made to create a sensing layer which can allow for multiple shots on an FBG.

# REFERENCES

[1] B. Larsen, K. Netto, and B. Aisbett, “The effect of body armor on performance, thermal stress, and exertion: a critical review.,” *Mil. Med.*, vol. 176, no. November, pp. 1265–73, 2011.

[2] Board on Army Science and Technology, *Testing of Body Armor Materials: Phase III*. 2012.

[3] N. M. A. Board, “High-Performance Fiber Technology,” in *High Performance Structural Fibers for Advanced Polymer Matrix Composites*, 2005, pp. 6–17.

[4] E. Hanlon and P. Gillich, “Origin of the 44-mm Behind-Armor Blunt Trauma Standard,” *Mil. Med.*, vol. 177, no. 3, 2012.

[5] P. V Cavallaro, “Soft Body Armor: An Overview of Materials, Manufacturing, Testing, and Ballistic Impact Dynamics.” 2011.

[6] Y. Duan, M. Keefe, T. A. Bogetti, and B. Powers, “Finite element modeling of transverse impact on a ballistic fabric,” *Int. J. Mech. Sci.*, vol. 48, no. 1, pp. 33–43, Jan. 2006.

[7] M. Pasquali, C. Terra, and P. Gaudenzi, “Analytical modelling of high-velocity impacts on thin woven fabric composite targets,” *Compos. Struct.*, vol. 131, 2015.

[8] B. A. Cheeseman and T. A. Bogetti, “Ballistic impact into fabric and compliant composite laminates,” *Compos. Struct.*, vol. 61, no. 1–2, pp. 161–173, 2003.

[9] M. P. Rao, Y. Duan, M. Keefe, B. M. Powers, and T. A. Bogetti, “Modeling the effects of yarn material properties and friction on the ballistic impact of a plain-weave fabric,” *Compos. Struct.*, vol. 89, no. 4, pp. 556–566, Aug. 2009.

[10] M. Karahan, A. Kuş, and R. Eren, “An investigation into ballistic performance and energy absorption capabilities of woven aramid fabrics,” *Int. J. Impact Eng.*, vol. 35, no. 6, pp.

499–510, Jun. 2008.

[11] P. K. PORWAL and S. L. PHOENIX, “Modeling system effects in ballistic impact into multi-layered fibrous materials for soft body armor,” *Int. J. Fract.*, 2005.

[12] D. Zhu, A. Vaidya, B. Mobasher, and S. D. Rajan, “Finite element modeling of ballistic impact on multi-layer Kevlar 49 fabrics,” *Compos. Part B Eng.*, vol. 56, 2014.

[13] X. Chen, F. Zhu, and G. Wells, “An analytical model for ballistic impact on textile based body armour,” *Compos. Part B Eng.*, vol. 45, no. 1, pp. 1508–1514, Feb. 2013.

[14] Y. Yang and X. Chen, “Study of energy absorption and failure modes of constituent layers in body armour panels,” *Compos. Part B Eng.*, vol. 98, pp. 250–259, Aug. 2016.

[15] L. Cannon, “Behind Armour Blunt Trauma - an emerging problem,” *J. R. Army Med. Corps*, vol. 147, no. MARCH 2001, pp. 87–96, 2001.

[16] C. R. Bass *et al.*, “Injury Risk in Behind Armor Blunt Thoracic Trauma,” *Int. J. Occup. Saf. Ergon.*, vol. 124, no. 4, pp. 429–442, 2006.

[17] R. N. Prather, C. L. Swann, and C. E. Hawkins, “Backface Signatures of Soft Body Armors and the Associated Trauma Effects.” 1977.

[18] D. P. Bentz, A. Forster, K. Rice, and M. Riley, “Thermal Properties and Thermal Modeling of Ballistic Clay Box,” *NISTIR 7840, U.S. Dep. Commer.*, 2011.

[19] National Institute of Justice, “Ballistic resistance of personal body armor 0101,” *Law Enforc. Correct. Stand. Test. Progr.*, p. 67, 2000.

[20] R. N. Prather and L. W. Metker, “Ballistic Test Matrix for Kevlar Material,” 1976.

[21] M. Nasr-Isfahani, M. Amani Tehran, and M. Latifi, “Simulation of ballistic impact on fabric armour using finite-element method,” *J. Text. Inst.*, vol. 100, no. 4, 2009.

[22] C. T. Lim, V. P. W. Shim, and Y. H. Ng, “Finite-element modeling of the ballistic impact

of fabric armor," *Int. J. Impact Eng.*, vol. 28, no. 1, pp. 13–31, 2003.

[23] A. Tabiei and G. Nilakantan, "Ballistic Impact of Dry Woven Fabric Composites: A Review," *Appl. Mech. Rev.*, vol. 61, no. 1, p. 010801, 2008.

[24] T. Goode, "Soft Body Armor Back Face Deformation with Ballistics Gel Backing," 2017.

[25] M. Kreuzer, "Strain measurement with fiber bragg grating sensors," *HBM, Darmstadt, S2338-1.0 e*, 2006.

[26] F. Seng *et al.*, "Split Hopkinson bar measurement using high-speed full-spectrum fiber Bragg grating interrogation," *Appl. Opt.*, vol. 55, no. 25, 2016.

[27] F. Seng *et al.*, "Dynamic back face deformation sensing with a single fiber Bragg grating."

[28] N. C. S. University, "Structure Scanner Picture.pdf." [Online]. Available: https://www.lib.ncsu.edu/devices/structure-3d-scanner.

[29] K. O. Hill and G. Meltz, "Fiber Bragg grating technology fundamentals and overview," *J. Light. Technol.*, vol. 15, no. 8, pp. 1263–1276, 1997.